

Suitability of post-Newtonian/numerical-relativity hybrid waveforms for gravitational wave detectors

Iana MacDonald

Canadian Institute for Theoretical Astrophysics, University of Toronto, Toronto, Ontario M5S 3H8, Canada

Samaya Nissanke

Jet Propulsion Laboratory, California Institute of Technology, 4800 Oak Grove Drive, Pasadena, California 91109
Theoretical Astrophysics 350-17, California Institute of Technology, Pasadena, CA 91125
Canadian Institute for Theoretical Astrophysics, University of Toronto, Toronto, Ontario M5S 3H8, Canada

Harald P. Pfeiffer

Canadian Institute for Theoretical Astrophysics, University of Toronto, Toronto, Ontario M5S 3H8, Canada

Abstract. This article presents a study of the sufficient accuracy of post-Newtonian and numerical relativity waveforms for the most demanding usage case: parameter estimation of strong sources in advanced gravitational wave detectors. For black hole binaries, these detectors require accurate waveform models which can be constructed by fusing an analytical post-Newtonian inspiral waveform with a numerical relativity merger-ringdown waveform. We perform a comprehensive analysis of errors that enter such “hybrid waveforms”. We find that the post-Newtonian waveform must be aligned with the numerical relativity waveform to exquisite accuracy, about 1/100 of a gravitational wave cycle. Phase errors in the inspiral phase of the numerical relativity simulation must be controlled to $\lesssim 0.1\text{rad}$. (These numbers apply to moderately optimistic estimates about the number of GW sources; exceptionally strong signals require even smaller errors.) The dominant source of error arises from the inaccuracy of the investigated post-Newtonian Taylor-approximants. Using our error criterium, even at 3.5-th post-Newtonian order, hybridization has to be performed significantly before the start of the longest currently available numerical waveforms which cover 30 gravitational wave cycles. The current investigation is limited to the equal-mass, zero-spin case and does not take into account calibration errors of the gravitational wave detectors.

PACS numbers: 04.25.D-, 04.25.dg, 04.25.Nx, 04.30.-w

1. Introduction

Coalescing black-hole binaries are amongst the most promising sources for the current and future gravitational wave (GW) detectors such as LIGO, Virgo, LCGT [1, 2, 3, 4] and LISA [5, 6, 7]. After several years of instrument upgrades, the next generation of ground-based interferometers should be operational within five years (~ 2015 -2016). At advanced sensitivities, currently predicted event rates for stellar mass binary black holes (BBH) with total masses $< 100M_{\odot}$ range from 0.4 to 1000 per year (with 20 being the “realistic” number given in [8]) detectable up to distances of \sim several Gpc. (Henceforth, for simplicity, we consider LIGO to be representative of all ground-based GW detectors.) In contrast, LISA will be sensitive to massive BBH systems with individual masses of $10^4 - 10^7M_{\odot}$ up to redshifts of ~ 20 .

In order to detect GWs and derive the emitting sources’ physical properties, accurate source modeling of predicted GWs is required in the form of a vast family of waveform templates. Analytical weak-field approximation methods such as the post-Newtonian (PN) expansion in general relativity accurately describe their inspiral prior to merger, whereas numerical relativity (NR) is used to model the merger of the two bodies in the strong-field regime. Both techniques have come to fruition over the last decade, e.g. the reviews [9, 10, 11, 12]. Because of the computational cost of numerical simulations ($\sim 100,000$ CPU-hours for long inspirals of generic precessing systems), current NR simulations cover $\lesssim 15$ orbits. These NR waveforms are then fused together with a waveform covering the earlier stage of the inspiral, calculated using high order PN expansions. Such fused waveforms are referred to as *hybrid* waveforms.

Hybrids play an important role in the construction of PN inspired phenomenological [13, 14] waveforms, which are intended for event detection. In addition, hybrids may guide the construction of easy-to-implement waveforms that are being developed for measurement purposes. Within the Ninja project [15, 16], moreover, GW data analysts search for hybrid waveforms embedded in detector noise of ground-based detectors to investigate efficiency of GW data-analysis pipelines. Finally, the Numerical Relativity and Analytical Relativity collaboration (NRAR) [17] aims to construct analytical waveform models that span the entire parameter space of spins and mass ratios. Such models then allow us to compute waveforms with little computational expense for any choice of parameters. Some of the waveform models pursued in this collaboration might involve hybrid waveforms. All these applications rest on sufficiently accurate hybrid waveforms, motivating our study.

Besides hybrid waveforms, analytical waveform models based on the effective-one-body (EOB) formalism are common, e.g. [18, 19]. EOB waveforms are a resummed extension of PN approximants, e.g. [20]. In this approach, one fits the EOB model directly against NR waveforms, without the intermediate step of constructing hybrid waveforms. Such fits, too, will be sensitive to errors in the NR waveforms. Conclusions about required accuracy of NR waveforms for hybrid waveforms may inform required accuracies for the NR waveforms that are used when fitting EOB models.

Both detection and measurement require hybrid waveforms to be of sufficient accuracy, to avoid a negative impact on the signal processing in noisy detector data. In conjunction with earlier work [21], Lindblom *et al.* [22] laid the foundations for accuracy standards for model waveforms. The formalism is applicable to all model waveforms (including PN only, NR only, and hybrids). In addition, though not considered in this work, Refs. [23, 24, 25] extend the original model waveform analysis

of Ref. [22] by incorporating instrument calibration errors and deriving more refined accuracy requirements within the time domain.

Based on Ref. [22] and complementary to recent investigations [26, 14, 27, 28], we implement waveform accuracy requirements that preserve detection efficiency and parameter estimation performance. We place bounds on the *norm* of the *modeling error* $\delta h_{\text{model}} = h_{\text{model}} - h_{\text{exact}}$, where h_{exact} is assumed to be some exact waveform (a solution of Einstein’s equations at infinite precision), and h_{model} is an approximate model waveform. Specifically, the error measure $\|\delta h\|/\|h\|$ translates to a normalized noise-weighted cross-correlation of the modeling error δh_{model} with itself, and is thus instrument-dependent, but distance-independent.

Our work computes this quantitative *accuracy measure* in order to assess different sources of error arising from hybrid waveforms for non-spinning, equal-mass binary black holes. Rather than emphasizing the immediate aim of event detection, we take a long-term perspective, and consider the ultimate accuracy requirements necessary for data-analysis once GW detections have become routine. The emphasis lies, therefore, on the optimal extraction of source characteristics from the observed waveforms. Due to the very nature of their construction, hybrids suffer from sources of error such as the type and location of matching the PN and NR waveforms, and the PN and NR waveforms themselves. For instance, PN methods rely on an expansion in powers of v/c (where v is the BBH’s typical orbital velocity and c is the speed of light)[‡], and result in an inspiral waveform with both PN amplitude and PN phase corrections. In addition, several different PN inspiral waveforms may be computed at a particular PN order because of differences when truncating Taylor expansions (commonly referred to as Taylor T1, Taylor T3, Taylor F2, etc., see e.g. Ref. [29]).

An immediate question that arises when constructing hybrids is where matching between their PN and NR waveforms should occur. This is of practical importance because of the computational expense incurred in producing NR waveforms. Stitching PN and NR waveforms as late as possible minimizes computational cost. However, PN waveforms, derived using approximate perturbative methods in general relativity, become increasingly inaccurate as merger is approached. We investigate here where best to match PN and NR waveforms. Other possible sources of error, all defined below and explored here within a unified framework, include numerical resolution, the extraction radius of NR waveforms, the accuracy and approximant of the PN waveform, the matching width, and the effect of error within the matching procedure itself. We also examine quantitatively how detection and measurement accuracies vary using different ground-based instrument noise curves, all of which have different regions of sensitivity.

This work thus provides a comprehensive quantitative measure of error for waveforms from several sources. The paper is organized as follows: Sec. 1.1 describes related earlier work and Sec. 1.2 introduces the notation used in this paper. Sec. 2 describes possible errors in hybrid waveforms and how to quantify them. Sec. 3 outlines our methodology: we begin with an explanation of the PN and NR waveforms in Secs. 3.1 and 3.2, of the hybridization process in Sec. 3.3, and of the computation of our error measures in Sec. 3.4. In Sec. 4, we present a detailed study of the different sources of error in hybrid waveforms. Sec. 5 presents our conclusions.

[‡] The notation 1PN corresponds to the formal $\sim 1/c^2$ level in a post-Newtonian expansion with respect to the Newtonian acceleration and gravitational wave flux (where c is the speed of light).

1.1. Previous work

Earlier works have examined similar aspects of detection and measurement errors of hybrid waveforms in the case of Initial and Advanced LIGO. Although the literature review presented here is far from complete, we chronologically outline four works which follow methodologies closely related to our study. As discussed in detail in Sec. 2, quantities in these works such as overlap, mismatch, faithfulness, effectualness and inaccuracy are related to our error measure $\|\delta h\|/\|h\|$. Throughout the rest of the paper, we will return to them to compare our results with their findings.

First, Buonanno *et al.* [26] compute overlaps between different time- and frequency-domain PN waveforms and EOB waveforms for four non-spinning binaries with specific masses (the systems are $(1.38, 1.42) M_\odot$, $(9.5, 10.5) M_\odot$, $(10, 1.4) M_\odot$ and $(4.8, 5.2) M_\odot$). The overlaps are maximized either over time- and phase-shifts (faithfulness), or over time- and phase-shifts and masses (effectualness). Ref. [26] does not consider hybrid or NR waveforms *per se*. Instead, it uses EOB waveforms that were *calibrated* with NR simulations. In the case of Initial, Enhanced and Advanced LIGO, Ref. [26] concludes that the majority of Taylor approximants (excluding TaylorT3 and TaylorEt) are sufficient for detection purposes for masses $< 12M_\odot$ whilst advocating the use of EOB for masses $> 12M_\odot$.

Second, whilst constructing a new set of phenomenological waveforms for aligned and anti-aligned spinning BBHs, Santamaría *et al.* [14] compute the normalized distance squared $(\|\delta h\|/\|h\|)^2$ (a quantity defined as the *inaccuracy*, see Ref. [28]) for hybrids constructed by matching PN and NR waveforms in the *frequency* domain. This differs from our study, where matching proceeds only in the *time* domain. The PN waveforms comprise Taylor T1, Taylor T4, or Taylor F2, and the NR waveform in the non-spinning case is an earlier version of the SpEC waveform used here. Santamaría *et al.* [14] determine the matching region itself by means of a least-squares fit between PN and NR waveform. This results in a matching region which extends very close to merger, $M\omega \in [0.063, 0.126]$. Quantifiable error sources are given by numerical resolution and by the differences between Taylor T1, Taylor T4 or Taylor F2 hybrids. Ref. [14] concludes that the PN truncation error, represented by the difference between different PN approximants, provides the largest source of error.

Third, and most similar to the approach followed here, Hannam *et al.* [27] aim to determine the necessary length of NR waveforms for the construction of hybrid waveforms. Ref. [27] considers both the mismatch (minimized over time and phase-shifts with or without mass-optimization), equivalent to one minus the overlap, and the inaccuracy, $(\|\delta h\|/\|h\|)^2$. As in Ref. [14], Ref. [27] constructs hybrid waveforms for aligned- and anti aligned-spinning and non-spinning equal- and unequal-mass BBHs. Focusing on the non-spinning equal-mass case, they use PN Taylor T1 and Taylor T4 approximants, and an earlier variant of the NR waveform used here. Ref. [27] computes quantitative error measures by comparing hybrids constructed from Taylor T1 and Taylor T4 with different matching frequencies between 0.045 and 0.09, using an Advanced LIGO noise curve with a low-frequency cut-off at 20Hz. Ref. [27] focuses on the near-term goal of event detection, and therefore places significantly weaker accuracy constraints on the hybrid waveforms. Nevertheless, Ref. [27] concludes that PN variants and PN order contribute the largest sources of error.

Finally, Damour *et al.* [28] compute the effectualness and inaccuracy between PN, phenomenological and EOB waveforms for non-spinning unequal-mass systems. The PN waveform used is Taylor F2, a frequency domain approximant also employed in

Santamaría *et al.* [14]. Similar to Ref. [26], they do not consider NR waveforms and use an analytical Advanced LIGO noise curve [13]. Indeed, although similar in approach, Ref. [28] investigates different sources of errors in hybrid and EOBNR waveforms than the present work. Ref. [28] finds that frequency-domain PN hybrids and phenomenological waveforms, unlike their EOBNR counterparts, fail to satisfy the minimal required accuracy standard for total mass $M < 75M_{\odot}$, even for moderately low signal-to-noise ratio.

Shortly after the present article was submitted, a further study was performed by Boyle [30]. This reference studies length requirements of Taylor-PN approximants hybridized with EOB waveforms.

Our work explores sources of errors in hybrid waveforms, aspects of which were investigated by these earlier works [26, 14, 27, 28], within a uniform framework. In agreement with others, we find that the dominant source of error is due to the uncertainty between PN Taylor-approximants. Indeed, using our error criteria, even at the highest available PN accuracy, we show that NR waveforms must be longer than the currently available 30 GW cycles when constructing hybrids with Taylor PN approximants in the non-spinning equal mass BBH case.

1.2. Notation

Throughout the paper, we use the following notation:

- h_{exact} represents the *exact* waveform.
- h_{PN} and h_{NR} denote the *post-Newtonian* and *numerical relativity* waveforms respectively.
- h_{H} specifies a *hybrid* waveform.
- ρ refers to the signal-to-noise ratio (SNR).
- $\|\delta h\|/\|h\|$ is our error measurement of the difference between a reference and trial hybrid.
- \mathcal{O} is the overlap between two waveforms.
- \mathcal{M} is the mismatch between two waveforms, defined as $1 - \mathcal{O}$.
- ρ_{eff} is the SNR divided by a detection safety factor ϵ , and corrected for a network of detectors. Its inverse $1/\rho_{\text{eff}}$ is the upper limit for our error calculations.

2. Quantifying errors

As mentioned in the introduction, hybrid waveforms are susceptible to a wide range of possible errors. We consider evolution of a binary black hole system with certain given intrinsic parameters like mass ratio, spins, and orbital elements. If one were able to solve Einstein's equations to infinite precision, one would obtain the *exact* waveform $h_{\text{exact}} = h_{\text{exact}}(t)$ emitted by this system. For simplicity, we will only consider the dominant $l = 2$, $m = 2$ of the gravitational radiation.

Numerical relativity computes an approximation to h_{exact} , which we shall denote h_{NR} . The NR waveform h_{NR} may differ from the exact waveform h_{exact} for a variety of reasons, among them:

- (i) *Truncation error* due to finite numerical resolution. As numerical resolution is increased, the solution will converge to the solution of the underlying continuous initial-boundary-value problem.

- (ii) This continuous initial-boundary-value problem may differ from the realistic physical system, for instance, due to imperfect outer boundary conditions.
- (iii) Gravitational radiation extracted at a finite radius may differ from the real waveform at future null infinity, due to ambiguities in the definition of gravitational radiation at finite radius, and imperfect wave extraction algorithms.
- (iv) Initial data for the numerical simulation may not precisely correspond to the desired situation; for instance, the orbital eccentricity of the simulation might differ slightly from the desired value.

This list is incomplete. We further emphasize that many possible sources of error for h_{NR} do *not* converge away with increased numerical resolution, such as, for example, the last three items in the list above.

The most striking difference between h_{NR} and h_{exact} is the length. The exact waveform is infinitely long, with an infinite number of gravitational wave cycles before merger. In contrast, the NR waveform has a finite number of cycles. Therefore, it is customary to attach a PN inspiral h_{PN} at the beginning of h_{NR} , resulting in a *hybrid* waveform h_{H} of sufficient length to encompass the entire sensitivity band of the detector within a desired mass-range.

Hybridization introduces several new potential sources of difference between h_{exact} and the hybrid waveform h_{H} :

- (v) PN theory is in itself only an approximation to full general relativity; hence h_{PN} will differ from h_{exact} by some amount, which increases with decreasing separation of the binary. The accuracy of h_{PN} also depends on the PN order of the approximant.
- (vi) One must identify and match parameters like masses and spins in the PN formalism with those in the numerical simulation[§].
- (vii) The matching between h_{PN} and h_{NR} is very sensitive to certain seemingly small errors in h_{PN} or h_{NR} .

To illustrate possible issues related to the matching, consider a particularly simple hybridization procedure. This procedure chooses a reference frequency x_0 and time-shifts h_{NR} and h_{PN} such that both waveforms pass through this frequency at the same time. Here, we parameterize frequency by the PN-frequency parameter [9] $x = (M\Omega)^{2/3}$, where M is the total mass of the binary and Ω its orbital frequency. The sensitivity arises because the inspiral rate \dot{x} decays very rapidly with decreased orbital frequency (i.e. increased separation), with $\dot{x} \propto x^5$ during the inspiral at lowest PN order. Therefore, a small frequency-error δx in one of the two waveforms that are to be matched results in an error

$$\delta t = \frac{\delta x}{\dot{x}} \propto \frac{\delta x}{x^5} \quad (1)$$

in the time-offset necessary to align the two waveforms with each other. The term x^{-5} causes the sensitivity of the matching between PN waveform and NR waveform. Matching typically occurs at frequencies $x \sim 0.1$. Whether or not δt increases or decreases as one pushes the matching to lower frequency depends on how quickly δx decreases with earlier matching. Let us consider the error due to the (unknown) 4PN

[§] This point was discussed in great detail in [14]; here we simply choose masses and spins in the PN waveform to be equal to those in the NR simulation.

term contribution. As a function of time-to-coalescence Θ , the 4PN term contributes an amount

$$\delta x_{4\text{PN}} \propto \Theta^{-5/4} \propto x^5 \quad (2)$$

to the frequency. The first proportionality arises from the PN expansion of x as a function of Θ , (cf. [9]), whereas the second proportionality arises from the Newtonian relation $x \propto \Theta^{-1/4}$. Substituting Eq. (2) into Eq. (1), we see that the unknown 4PN coefficient contributes an error δt independent of the matching frequency.

As a second example, let us consider the orbital phase: the (unknown) 4PN term of the orbital phase, expressed as a function of frequency x is

$$\Phi_{4\text{PN}} \propto x^{3/2} \propto \Theta^{-3/8}. \quad (3)$$

The impact of unknown higher-order PN terms on the orbital phase, therefore, decays with smaller frequency x . However, this decrease is *very slow*: To reduce the effect of $\Phi_{4\text{PN}}$ by a factor of 2, one has to terminate the PN waveform by a factor $2^{8/3} \approx 6.4$ earlier in time, with a corresponding increase of the length of the NR simulation which takes the binary to merger. Because of the high computational cost of an NR simulation, increasing its length by large factors like 6.4 is hardly practical. Furthermore, the numerical waveform h_{NR} also contributes potential issues for matching at earlier times. Widely separated binaries are particularly difficult to simulate numerically, due to the small energy flux which drives the inspiral, and due to the long wavelength of the gravitational radiation. Moreover, the first portion of numerical simulations tends to be noisy due to junk radiation [34, 35, 36, 37] arising from the initial conditions.

We see, therefore, that there are a wide variety of effects which might cause h_{H} to differ from the desired h_{exact} . Whether such differences are relevant will depend on the application of the waveforms. We focus here on applications to GW detection and, in particular, measurement. The sensitivity of GW detectors is frequency dependent (see Fig. 1), and therefore, the importance of errors will depend on their frequency dependence. Because BBH waveforms are invariant under a rescaling of mass, *one* PN-NR hybrid waveform h_{H} represents binaries of any total mass M for a given mass ratio. However, depending on the mass M , different portions of h_{H} are in the most sensitive frequency range of the detector. Furthermore, waveforms are typically used in matched filtering, e.g. [38, 39], a technique that allows for time- and phase-shifts of the gravitational waveform. Thus, those components of the difference $h_{\text{H}} - h_{\text{exact}}$ that can be represented by a time- or phase-shift are not relevant.

Let us assume that the exact signal h_{exact} and the computed hybrid waveform h_{H} are so close to each other that the Taylor-series expansions used implicitly in the Fisher-matrix formalism are valid. We denote

$$\delta h \equiv h_{\text{H}} - h_{\text{exact}}, \quad (4)$$

where δh is the difference between the hybrid and exact waveform when optimally aligned in phase and time. To introduce some key concepts, we shall assume that we know δh . Miller [21] and Lindblom *et al.* [22] pointed out that the key quantity for assessing the importance of errors is the inner product $\|\delta h\|^2 \equiv \langle \delta h, \delta h \rangle$, where

$$\langle g, h \rangle = 2 \int_0^\infty df \frac{\tilde{g}^*(f)\tilde{h}(f) + \tilde{g}(f)\tilde{h}^*(f)}{S_n(f)}, \quad (5)$$

|| Implicit time-stepping techniques [31, 32, 33] are expected to reduce this limitation.

¶ A commonly made assumption in gravitational wave data-analysis.

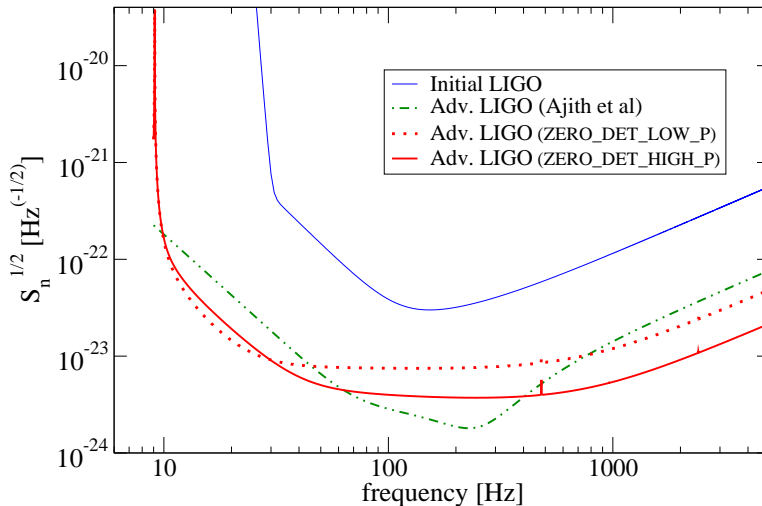


Figure 1. LIGO noise curves used in our analysis. We predominantly use ZERO_DET_HIGH_P, as predicted for Advanced LIGO [40]. ZERO_DET_LOW_P is the Advanced LIGO sensitivity curve with a lower-powered laser. In Sec. 4.5, we compare to two earlier noise curves, Initial LIGO, and an earlier Advanced LIGO noise curve used by Ajith *et al.* [13]. The wider bandwidth of ZERO_DET_HIGH_P places more stringent phase coherency on waveform templates.

with $\tilde{g}(f)$ and $\tilde{h}(f)$ the Fourier transforms of two waveforms $g(t)$ and $h(t)$. $S_n(f)$ denotes the (one-sided) power spectral density matrix,

$$S_n(f) = 2 \int_{-\infty}^{\infty} d\tau e^{2\pi i f \tau} C_n(\tau), \quad f > 0, \quad (6)$$

where $C_n(\tau)$ is the noise correlation matrix for zero-mean, stationary noise. The noise spectra employed in this paper are shown in Fig. 1. We will generally focus on the noise curve ZERO_DET_HIGH_P, the highest-sensitivity design goal for Advanced LIGO [40]. This configuration is sensitive over a wider bandwidth than the Initial LIGO, and earlier estimates for Advanced LIGO, used, for example, in Refs. [13] and [28]. Therefore, the PN inspiral and the NR late inspiral–merger–ringdown are simultaneously in band for a larger range of total binary masses than for previous noise curves. For the earliest matching frequency considered here ($M\omega = 0.038$), the matching region will be in Advanced LIGO’s sensitivity band (defined here as 10Hz to 1000Hz) for total masses between about $1.2M_\odot$ and $125M_\odot$.

When

$$\|\delta h\| < 1, \quad (7)$$

a detector with noise-spectrum $S_h(f)$ cannot experimentally distinguish between the waveforms h_H and h_{exact} . Therefore, h_H is a suitable substitute for h_{exact} for parameter estimation in this case. The inequality (7) is sufficient but not necessary. For instance, if δh is orthogonal to the signal manifold, its impact on parameter estimation is diminished.

Event detection genenerally places less restrictive demands on the accuracy of the waveforms h_H . A sufficient criterion is given by Lindblom *et al.* [22],

$$\|\delta h\| < \sqrt{2\varepsilon_{\text{max}}} \rho, \quad (8)$$

where the signal-to-noise ratio (SNR) $\rho = \|h_{\text{exact}}\|$. The dimensionless number ε_{max} depends on the reduction in SNR (and thus event rate) one is willing to tolerate during event detection. For typical template placement in Initial LIGO data-analysis, Lindblom *et al.* suggest $\varepsilon_{\text{max}} = 0.005$. These numbers may have to be reconsidered for Advanced LIGO data analysis [41], based on the cost of using a template bank (which depends on the number of templates) relative to the cost of computing the templates in the first place.

For non-spinning equal mass BBHs, the waveforms h_{exact} and h_{H} depend trivially on two parameters: the luminosity distance and total redshifted mass. The luminosity distance to the source is introduced as an overall scaling of the amplitude. For BBHs (as considered here), the total redshifted mass comes into play only via trivial rescalings of amplitude and time (i.e. frequency). The dependence on distance and mass carries forward into $\|\delta h\|$, complicating evaluation of Eqs. (7) and (8). The distance dependence can be removed through division by the signal-to-noise-ratio, i.e. by computing

$$\frac{\|\delta h\|}{\rho}. \quad (9)$$

In terms of this quantity, the accuracy requirements become⁺

$$\frac{\|\delta h\|}{\|h\|} < \begin{cases} 1/\rho_{\text{eff}}, & \text{parameter estimation} \\ \sqrt{2\varepsilon_{\text{max}}}. & \text{event detection} \end{cases} \quad (10)$$

The square of the left-hand-side of Eq. (10) is called *inaccuracy functional* by Damour *et al.* [28]. Because of our emphasis on numerical errors, we prefer to define this quantity without the square, so that $\|\delta h\|/\|h\|$ will be proportional to the numerical errors. This has the added benefit that the right-hand side is proportional to the inverse of the signal-to-noise ratio and not its inverse square.

For the parameter estimation limit in Eq. (10), we have replaced the single detector SNR ρ by an *effective SNR* ρ_{eff}^* . This effective SNR allows us to incorporate a safety factor $\varepsilon < 1$, as recently argued by Damour *et al.* [28]. The safety factor reduces the impact of waveform errors δh to a fraction ε of the effects of the detector noise; Damour *et al.* [28] suggest $\varepsilon \sim 1/3 - 1/2$, in light of the fact that it is easier to calculate more accurate waveform templates than to enhance the sensitivity of the GW detectors. Furthermore, ρ_{eff} can absorb the impact of a *network* of detectors. In a network of detectors with Gaussian, independent noise, the overall network SNR is the root-square-sum of the detector SNRs. Thus, though GW detectors have non-Gaussian noise, one can still get a rough sense of the requirements for a coherent network of N individual detectors by incorporating a factor \sqrt{N} into ρ_{eff} ,

$$\rho_{\text{eff}} = \varepsilon^{-1} \sqrt{N} \rho. \quad (11)$$

Let us consider reasonable values for ρ_{eff} . Our focus is on parameter estimation, i.e. we would like to obtain results that guarantee sufficiently accurate hybrids for most Advanced LIGO events. In realistic scenarios, Advanced LIGO may be seeing 20 binary black holes per year [8]. Because LIGO is volume limited, most of these

⁺ For event detection, it is irrelevant which template matches a certain physical signal h_{exact} , and reliable estimates of detection sensitivities require mismatch calculations optimizing over physical parameters like total mass or mass-ratio. We do not consider such optimizations in this paper, and therefore Eq. (10) gives only an approximate, conservative indication of requirements for event detection.

* Lindblom *et al.*'s original bound can be recovered by setting $\varepsilon = 1$.

events will have an SNR close to the detection threshold, with the number of stronger events decaying like ρ^{-3} . The strongest event in a year will have a SNR larger by a factor $\sim 20^{1/3} = 2.7$ than the detection threshold, placing it around SNR of ≈ 20 . Including a safety factor $\varepsilon = 1/2$, one arrives at $\rho_{\text{eff}} = 40$. Accounting for 3 detectors increases this bound to $\rho_{\text{eff}} = 40\sqrt{3} \approx 70$ and for 5 detectors to $\rho_{\text{eff}} = 40\sqrt{5} \approx 90$. Using the optimistic event rate estimate of 1000/yr [8] instead of the realistic rate of 20/yr, increases the largest expected SNR's by a further factor $(1000/20)^{1/3} \approx 3.7$ to $\rho_{\text{eff}} \approx 250$. To cover this range of possibilities, we will indicate $\rho_{\text{eff}} = 40$ and $\rho_{\text{eff}} = 100$ in the plots below. In addition, the event detection limit of Eq. (10), $\sqrt{2\varepsilon_{\text{max}}} \approx 0.1$, can be rewritten in terms of $\rho_{\text{eff}} = 10$. We also indicate this bound in our figures.

The dependence of $\|\delta h\|$ and $\|\delta h\|/\|h\|$ on the total mass can be taken into account by plotting $\|\delta h\|/\|h\|$ as a function of total mass. Such a plot gives insight into suitability of h_{H} for *both* event detection and parameter estimation; if $\|\delta h\|/\|h\|$ is below $\sqrt{2\varepsilon_{\text{max}}} \sim 0.1$ for certain masses, criterion (8) is satisfied, and h_{H} is suitable for event detection in that mass-range. The value of $\|\delta h\|/\|h\|$ as a function of mass gives the (inverse) signal-to-noise ratio, up to which h_{H} is suitable for parameter estimation. When a signal at a certain SNR ρ_{obs} is observed, the plot allows one to verify whether $\|\delta h\|/\|h\| < \varepsilon/\rho_{\text{obs}}$. If this inequality is satisfied, event characterization can proceed without delay; otherwise, more accurate waveforms h_{H} need to be computed for optimal event characterization.

So far, we have assumed knowledge of the exact solution h_{exact} , which, in practice, one does not know. Instead, we will below compute differences $\delta h = g - h$ between two hybrid waveforms g and h , where we consider the “superior” of the two hybrid waveforms as a substitute for h_{exact} . Thus, we will usually consider

$$\frac{\|\delta h\|}{\|h\|}. \quad (12)$$

Replacing the denominator of Eq. (12) by $\|g\|$, or by $\|g\|^{1/2}\|h\|^{1/2}$ changes Eq. (12) only by terms of higher order in δh and is therefore irrelevant. We will, therefore, consider Eq. (12) as a measure of the error of the “inferior” of the two waveforms g , h . In doing so, it is important that one of the waveforms is clearly more accurate than the other, otherwise Eq. (12) would simply measure the difference between two poor-quality waveforms (and such a difference can be arbitrarily small, if the two poor-quality waveforms happen to be near each other). We will discuss this point in more detail below.

The error measure $\|\delta h\|/\|h\|$ can be expressed in terms of the overlap \mathcal{O} and the mismatch $\mathcal{M} = 1 - \mathcal{O}$. The overlap between two waveforms g and h is defined as

$$\mathcal{O} = \frac{\langle g, h \rangle}{\sqrt{\langle g, g \rangle \langle h, h \rangle}} = \frac{\langle h + \delta h, h \rangle}{\sqrt{\langle h + \delta h, h + \delta h \rangle \langle h, h \rangle}}. \quad (13)$$

By Taylor expanding the denominator, we find:

$$\mathcal{O} = 1 - \frac{1}{2} \frac{\|\delta h\|^2}{\|h\|^2} + \frac{1}{2} h_{\parallel}^2 + \mathcal{O}(\delta h^3), \quad (14)$$

and

$$\frac{\|\delta h\|}{\|h\|} = \sqrt{2\mathcal{M} + h_{\parallel}^2} + \mathcal{O}(\delta h^2). \quad (15)$$

Here, h_{\parallel} is the normalized projection of δh onto h ,

$$h_{\parallel} = \frac{\langle \delta h, h \rangle}{\langle h, h \rangle} + \mathcal{O}(\delta h^2). \quad (16)$$

Normalizing Eq. (16) by $\|g\|^2$ instead of $\|h\|^2$ merely affects higher order terms. The quantity h_{\parallel} represents an overall rescaling between h and g ; if $g = (1 + \gamma)h$ for some constant γ , then $h_{\parallel} = \gamma$.

Eq. (15) relates our error measure $\|\delta h\|/\|h\|$ to the more widely used mismatch \mathcal{M} . The major difference is that $\|\delta h\|/\|h\|$ is also sensitive to an overall rescaling of the waveform, represented by h_{\parallel} , whereas \mathcal{M} is not. Waveforms h are high-dimensional vectors either in the time-, or frequency-domain, and the quantity h_{\parallel} only measures one dimension of this high-dimensional vector space. If one assumes errors that have components in many dimensions, and consequently neglects h_{\parallel} , then Eq. (15) simplifies to

$$\|\delta h\|/\|h\| = \sqrt{2\mathcal{M}}. \quad (17)$$

This relationship has also been noted in [22, 14, 27, 42].

When we compute $\|\delta h\|/\|h\|$ in subsequent sections, we always introduce a relative time- and phase-shift between g and h in order to minimize $\|\delta h\|/\|h\|$ and the mismatch \mathcal{M} , but we do not modify any other parameters of the waveform (such as the total mass). Thus, our analysis tests faithfulness [29]. A more appropriate error limit for detection is the *effectualness* where the error is minimized over the intrinsic parameters of the system, that is, the total mass in an equal-mass, non-spinning binary. Thus, our upper error limit of $\rho_{\text{eff}} = 10$ for detection is very conservative.

Finally, we note that the analysis presented here is not the first one in this spirit. Mismatches or $\|\delta h\|/\|h\|$ between various pairs of waveforms have been calculated before, for instance between purely numerical waveforms in the Samurai project [43], between analytical waveform models by Damour *et al.* [28], and also between hybrid waveforms [14, 27]. Our focus is a comprehensive and unified study of many error sources that enter hybrid waveforms, concentrating on parameter estimation.

3. Methodology

3.1. Post-Newtonian waveforms

The PN approximation in General Relativity relies critically on assumptions of weak field and of the source’s internal slow motion. It is characterized by the PN parameter $\epsilon \sim (v/c)^2 \sim (M/r)$, where M is the characteristic mass of the system and v the magnitude of the relative velocity. Construction of PN templates requires modeling both the local conservative dynamics of the system and the generation of its gravitational waves. The current state-of-the-art accuracy in both the gravitational wave generation and the description of the system’s local dynamics is 3.5PN in the case of non-spinning quasi-circular comparable mass inspiralling compact binaries (see Blanchet [9] and references therein for a detailed review). In the case of spinning inspiralling compact binaries, the amplitude-complete GW templates have been computed to 1.5PN order [44]. Following standard notation, n PN describes the n -th PN order in the phase, and “PN approximant n/m ” specifies the n -th and m -th PN corrections in the phase and amplitude respectively.

Standard formulae exist for PN gravitational polarization waveforms $h_{+}(t)$ and $h_{\times}(t)$ of quasi-circular orbits, which depend on the source’s location with respect to some observer. Usually, NR waveforms are decomposed into spherical harmonics and often only the dominant (2,2) mode is considered. This is the case with the set of NR simulations we use, and consequently, we will only need the (2,2) mode of the PN

approximant [45]:

$$\begin{aligned}
h_{(2,2)} = & -2\sqrt{\frac{\pi}{5}}\frac{GM}{c^2R}e^{-2i\Phi}x\left\{1 - \frac{373}{168}x + \left[2\pi + 6i\ln\left(\frac{x}{x_0}\right)\right]x^{3/2} - \frac{62653}{24192}x^2 \right. \\
& - \left[\frac{197}{42}\pi + \frac{197i}{14}\ln\left(\frac{x}{x_0}\right) + 6i\right]x^{5/2} + \left[\frac{43876092677}{1117670400} + \frac{99}{128}\pi^2 - \frac{428}{105}\ln x \right. \\
& \left. \left. - \frac{856}{105}\gamma - \frac{1712}{105}\ln 2 - 18\ln^2\left(\frac{x}{x_0}\right) + \frac{428}{105}i\pi + 12i\pi\ln\left(\frac{x}{x_0}\right)\right]x^3\right\}, \quad (18)
\end{aligned}$$

where the PN invariant velocity parameter is $x \equiv (M\Omega(t))^{2/3}$, $\Omega(t)$ is the orbital frequency and $\Phi(t) \equiv \int_0^t \Omega(t')dt'$ is the orbital phase. The parameter $\ln x_0 \equiv \frac{11}{18} - \frac{2}{3}\gamma + \frac{2}{3}\ln\left(\frac{GM}{4bc^3}\right)$ is a constant frequency scale which depends on the freely specifiable time parameter b . The latter characterizes the timescale at which the gravitational wave tail contributions enters the polarization waveforms. We choose $b = 1$.

Evaluation of (18) requires expressions for $x(t)$ and $\Phi(t)$. We will investigate the Taylor approximants TaylorT1, TaylorT3 and TaylorT4 (as defined in [46] and references therein). They are all completed by solving the energy-balance equation:

$$\frac{dE}{dt} = -\mathcal{L}, \quad (19)$$

where the GW flux at infinity \mathcal{L} is balanced by the change in the orbital binding energy $E(t)$ of the binary. The TaylorT approximants differ from each other by how higher-order PN terms are truncated in $E(t)$ and \mathcal{L} when implementing (19). In particular, TaylorT1 and TaylorT4 are solved by numerically integrating coupled sets of ordinary differential equations (see (35-36) and (45-46) in [46] respectively and [29, 47]), whereas analytical expressions exist for TaylorT3 (see (43)-(46) in [46] and [9]). Many previous studies have established that for equal-mass, non-spinning binaries the TaylorT4-approximant happens to agree very closely with the full numerical solution of Einstein's equations [48, 49, 46, 50]. There is, however, no *a priori* reason why TaylorT4 should perform better than TaylorT1 or TaylorT3. So that our results are as representative as possible, we therefore investigate several Taylor approximants (TaylorT1, T3, T4). By doing so, we achieve conservative estimates of how long NR simulations must be. We expect that our results are unaffected by accidental agreement of TaylorT4 for the specific configuration under study, so that our results will carry over to other parameter configurations where no exceptionally good PN approximant is known.

We start the PN waveforms at an initial orbital frequency of $M\Omega = 7.5 \times 10^{-4}$, resulting in a waveform of duration $\sim 1.7 \times 10^7 M$ containing ~ 6500 GW cycles to merger. The low starting frequency ensures an initial gravitational wave frequency of 10 Hz at $M = 5M_\odot$, so that the constructed hybrid waveforms cover the entire frequency band of the Advanced LIGO detectors for $M \geq 5M_\odot$.

3.2. Numerical Relativity Waveforms

In this paper, we focus on equal-mass non-spinning BBHs. We use a waveform generated with the *Spectral Einstein Code* SpEC [51]. The initial data is identical to that used in [46, 52], resulting in an inspiral lasting about 16 orbits at an initial orbital eccentricity of $\sim 5 \times 10^{-5}$. The techniques for the evolution are a refinement of those presented in [46, 52]. Specifically, the gauge source functions are rolled off to

zero early in the evolution, so that the inspiral proceeds in the harmonic gauge. The constraint-damping parameters are those described in [53], which reduce the impact of junk radiation. The merger was performed with a refinement of the techniques described in [54].

3.3. Construction of hybrid waveform

Construction of a hybrid waveform $h_H(t)$ from a PN waveform $h_{\text{PN}}(t)$ and NR waveform $h_{\text{NR}}(t)$ requires first that we align the waveforms with a relative time- and phase-shift, and then join them smoothly together. We begin by choosing a GW frequency interval of width $\delta\omega$ centered at frequency ω_m ,

$$\omega_m - \frac{\delta\omega}{2} \leq \omega \leq \omega_m + \frac{\delta\omega}{2}, \quad (20)$$

in which we perform the matching between NR and PN. During the inspiral, the gravitational wave frequency $\omega(t) = d\phi(t)/dt$ is continuously increasing, so (20) translates into a time-interval $t_{\text{min}} < t < t_{\text{max}}$. Here, $\phi(t)$ represents the phase of the (2,2) mode of the gravitational radiation.

The PN waveform $h_{\text{PN}}(t; t_c, \Phi_c)$ incorporates naturally the coalescence parameters t_c and Φ_c representing the time and phase freedom. We determine the parameters t'_c and Φ'_c by minimizing the GW phase difference in the matching interval $[t_{\text{min}}, t_{\text{max}}]$,

$$t'_c, \Phi'_c = \underset{t_c, \Phi_c}{\text{minloc}} \int_{t_{\text{min}}}^{t_{\text{max}}} (\phi_{\text{PN}}(t; t_c, \Phi_c) - \phi_{\text{NR}}(t))^2 dt. \quad (21)$$

The hybrid waveform is then constructed in the form

$$h_H(t) \equiv \mathcal{F}(t)h_{\text{PN}}(t; t'_c, \Phi'_c) + [1 - \mathcal{F}(t)]h_{\text{NR}}(t), \quad (22)$$

where $\mathcal{F}(t)$ is a blending function defined as

$$\mathcal{F}(t) \equiv \begin{cases} 1, & t < t_{\text{min}} \\ \frac{1}{2} \left(1 + \cos \frac{\pi(t-t_{\text{min}})}{t_{\text{max}}-t_{\text{min}}} \right), & t_{\text{min}} \leq t < t_{\text{max}} \\ 0. & t \geq t_{\text{max}} \end{cases} \quad (23)$$

Several other hybrid procedures have been proposed. Similar to our method, Hannam *et al.* and Ajith *et al.* [27, 13] match in the time domain, although they employ different blending functions (e.g., Eq. (4.11) in [13]). Both Santamaría *et al.* [14] and Damour *et al.* [28] match in the frequency domain using a χ^2 fit, and invoke different blending functions. Earlier hybrids were matched at a single frequency [46, 50]. We have experimented with minimizing the phase and amplitude difference when determining time and phase offset. Specifically, we replaced the integrand of (21) by $|h_{\text{PN}} - h_{\text{NR}}|^2$ using the complex (2,2) modes. We did not notice any significant change when using this different alignment scheme.

3.4. Computation of $\|\delta h\|/\|h\|$

We compute Fourier transforms of waveforms with standard Fast Fourier Transforms, rescaling the geometric units in which the hybrid waveforms are given to the desired physical mass. In order to reduce the Gibbs phenomenon, we multiply the time-domain waveform with a windowing function $w(t)$ before computing the Fourier transform. We tried two windowing functions, the Hann (or cosine squared) window [55] and the more

recent Planck-taper window function [56]. Our results did not differ noticeably when using the different windowing functions, and so the Planck-taper window [56] is used since it quickly goes to zero outside the window bounds:

$$w(t) = \begin{cases} 0, & t \leq t_1 \\ [e^{y(t)} + 1]^{-1}, & t_1 < t < t_2 \\ 1, & t_2 \leq t \leq t_3 \\ [e^{z(t)} + 1]^{-1}, & t_3 < t < t_4 \\ 0, & t_4 \leq t, \end{cases} \quad (24)$$

where $y(t) = (t_2 - t_1)/(t - t_1) + (t_2 - t_1)/(t - t_2)$ and $z(t) = -(t_3 - t_4)/(t - t_3) + (t_3 - t_4)/(t - t_4)$. The interval $[t_1, t_2]$ is chosen to cover the first five GW cycles of our hybrid waveform, whereas $[t_3, t_4]$ spans the very late ringdown.

Detector noise has a considerable effect on $\langle h, g \rangle$, since different parts of the waveform enter the detector band for different masses. When evaluating the noise weighted inner products in Eq. (5), we use the noise curves shown in Fig. 1, with the default being the Advanced LIGO ZERO_DET_HIGH_P curve.

Whenever we calculate $\|\delta h\|/\|h\|$ between two hybrid waveforms, we time- and phase-shift one of the two hybrid waveforms to maximize the overlap for each mass. We can write the Fourier transforms of the time- and phase-shifted waveform as follows:

$$\tilde{h}_{\Delta\phi, \Delta t} = (\tilde{h}_c \cos \Delta\phi + \tilde{h}_s \sin \Delta\phi) e^{2\pi i f \Delta t}. \quad (25)$$

The extremization over the phase-shift $\Delta\phi$ can be performed analytically. We define $a = \langle \tilde{h}_c, \tilde{g} \rangle$ and $b = \langle \tilde{h}_s, \tilde{g} \rangle$, where \tilde{h}_c is the Fourier transform of the real part of the first waveform, and \tilde{h}_s is the Fourier transform of its imaginary part. Thus,

$$\Delta\phi = \tan^{-1} \left(\frac{b}{a} \right), \quad (26)$$

which is the phase shift for maximum overlap if $[-\sin \Delta\phi - \cos \Delta\phi] < 0$ (otherwise π is added to the phase). Δt is found by using the Matlab minimization function `fminsearch`.

4. Results

In the following error analysis, we focus primarily on the upper limits of $\|\delta h\|/\|h\|$ for a single detector, corresponding to ρ_{eff} of 10 and 40 for detection and parameter estimation respectively. We do not discuss the upper error limit for multiple detectors, $\rho_{\text{eff}} \sim 100$, since none of our hybrid waveforms meet this error criterion, with the possible exception of those hybrids matched very early with a TaylorT4 waveform.

4.1. Effect of error in hybridization

During the hybridization procedure, as outlined in Section 3.3, the PN waveform must be aligned with the NR waveform by choosing t_c and Φ_c . The time shift t_c is difficult to determine, because a degeneracy between time and phase shift is only broken by the frequency evolution, which is very slow during the inspiral, cf. Sec. 2. On the other hand, minimization over the phase-shift Φ_c is trivial, because $\Phi_{\text{PN}}(t; t_c, \Phi_c) - \Phi_{\text{NR}}(t)$ in the integrand of Eq. (21) is linear in Φ_c . Therefore, we assume that errors in the determination of Φ_c are irrelevant, and focus on the time-offset by investigating

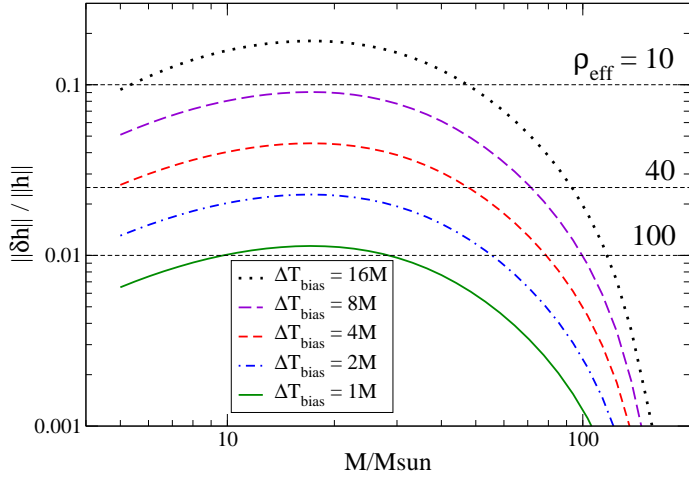


Figure 2. Effect of hybridization errors. We compare hybrid waveforms with alignment biased by ΔT_{bias} to the correctly hybridized waveforms. (Matching frequency $M\omega_m = 0.050$, highest-resolution NR waveform, and TaylorT3 PN waveform).

how accurately t_c must be determined. For this, we first construct a hybrid using the correct least-squares fit, resulting in the correct t'_c . We then construct a second hybrid by fixing the time-offset to $t'_c + \Delta T_{\text{bias}}$ and by performing the minimization over Φ_c only. We compute $\|\delta h\|/\|h\|$ between these two hybrids. All least-squares fits are performed over a frequency range of width $\delta\omega = 0.1\omega_m$ centered at frequency $M\omega_m = 0.05$.

Fig. 2 presents the results of this calculation. The error $\|\delta h\|/\|h\|$ decreases linearly with ΔT_{bias} ; this linear dependence is one advantage of using $\|\delta h\|/\|h\|$ over other measures, such as its square or the mismatch. Fig. 2 shows that even small errors in hybridization have a significant effect on the magnitude of $\|\delta h\|/\|h\|$. Time-shift errors larger than about 2M are unacceptable for parameter estimation at $\rho_{\text{eff}} \gtrsim 40$. In order to preserve some safety margin, we therefore conclude that the time-shift must be determined to better than 1M. (Strictly speaking, this estimate $\Delta T \lesssim 1M$ applies only for matching at a frequency $M\omega_m \approx 0.05$; this analysis would have to be repeated when matching earlier or later). This is a surprisingly tight bound; 1M is only $\sim 1/2000$ of the time-to-merger, and is only about 1% of a gravitational wave cycle.

Our primary goal is to utilize the bound on ΔT_{bias} when choosing the width of the matching interval in Sec. 4.2. However, to place this requirement $\Delta T_{\text{bias}} \lesssim 1M$ into perspective, consider the TaylorT2 PN approximant, which expresses time-to-merger as a power-series in orbital frequency. The 3.5PN-order contribution to the coalescence time for an equal-mass binary is given by (see [9] and references therein);

$$t_{3.5\text{PN}} = \frac{5M}{64} \frac{571496}{3969} \pi (M\Omega)^{-1/3} \approx 96M, \quad (27)$$

where we have used $M\Omega = M\omega_m/2 = 0.025$. The contribution $t_{3.5\text{PN}}$ is two orders of magnitude larger than the bound on ΔT_{bias} . Whilst it is difficult to translate time-offsets from PN contributions, this large disagreement immediately indicates that PN theory, even at 3.5PN order, might not be sufficiently accurate.

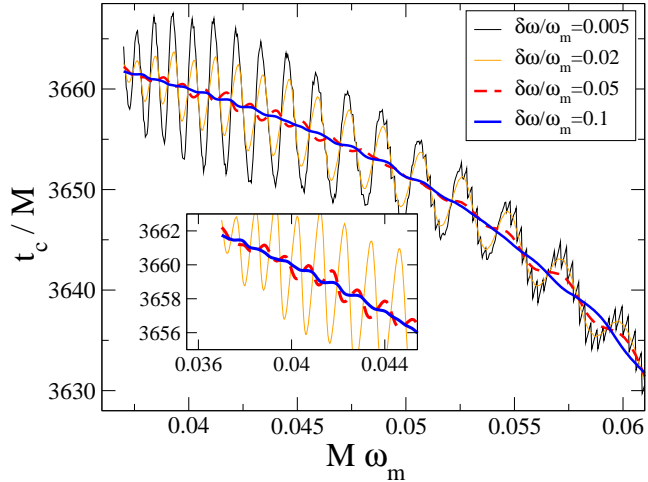


Figure 3. Effect of the width of matching window $\delta\omega/\omega_m$ on the best-fit time-shift t_c . For matching windows covering $\lesssim 1$ GW period ($\delta\omega/\omega_m \lesssim 0.02$), t_c is sensitive to small oscillations in the GW phase (thin lines). For windows covering $\gtrsim 1$ GW period, this sensitivity rapidly decreases (thick lines, also enlarged in the inset).

We note that Hannam *et al.* [27] also considered hybridization errors; this work compared three different hybridization schemes, and found that their difference is indistinguishable for certain SNRs. Our approach improves on this by explicitly giving conditions on the accuracy of t_c as in Fig. 2. This measure of hybridization errors might seem extremely specific because we only consider the errors due to the determination of t_c , however these error bounds apply to any time-domain hybridization procedure and to any effect that might give rise to an error in determination of t_c , like for instance a small eccentricity in the NR simulation.

4.2. Width of hybridization interval

The PN time- and phase-parameters t_c and Φ_c that align the PN waveform with the NR waveform are determined by a least-squares fit [see Eq. (21)]. The width of the matching interval $[t_{\min}, t_{\max}]$ influences the robustness of this fit for two reasons:

- (i) A small change δt_c in t_c is nearly degenerate with a small change $\delta\Phi_c$ in Φ_c , with $\delta\Phi_c \approx \omega_m \delta t_c / 2$. (The factor 1/2 arises because ω_m measures the frequency of the GW $l = 2, m = 2$ mode whereas Φ_c is the orbital phase). For circular Newtonian orbits, the degeneracy is perfect. For the general relativistic case, the degeneracy is broken only by the *evolution* during the hybridization interval, i.e. by the change in frequency ω . A longer fitting interval encompasses more evolution, and so helps to break the degeneracy.
- (ii) A longer fitting interval helps to “average out” undesirable features in the NR waveform. Such features might be caused by numerical artefacts like junk radiation or a slight residual eccentricity. In particular, matching over an interval much smaller than the orbital period will be susceptible to eccentricity effects, as discussed in Boyle *et al.* [46].

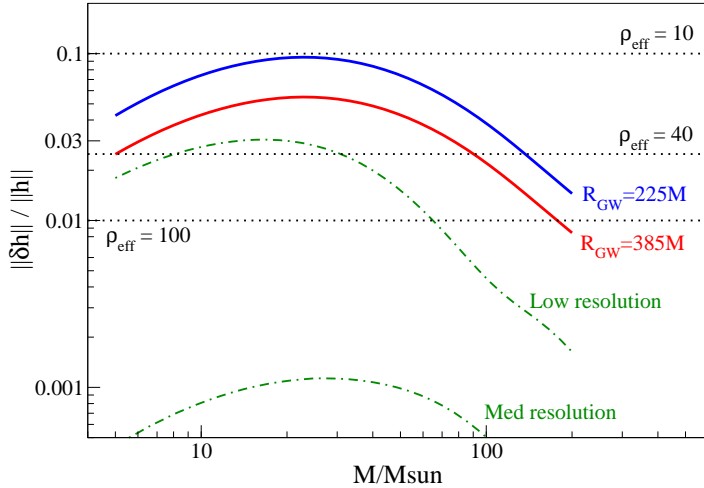


Figure 4. Effect of numerical errors. Shown is $\|\delta h\|/\|h\|$ between hybrid waveforms constructed with NR waveforms of different numerical resolution (dashed lines), and between hybrid waveforms of finite GW extraction radius R_{GW} vs. waveforms extrapolated to infinite extraction radius. (All hybrids matched at $M\omega = 0.042$ to a TaylorT3 PN waveform).

A robust fit Eq. (21) must be independent of small changes to the fitting interval. To test this, we compute many independent least-squares fits, over slightly shifted fitting intervals, parametrized by ω_m , the frequency in the middle of the fitting interval. Fig. 3 plots the resulting t_c for several different widths $\delta\omega$ of the matching interval.

For small $\delta\omega$, this figure shows significant variations in t_c . These variations arise because the fitting interval covers less than one GW period. Therefore, the fitting is sensitive to a small variation in the GW phase (of order 0.001 rad) present in the numerical data. As $\delta\omega/\omega \gtrsim 0.05$, this sensitivity rapidly decreases, as the fitting interval now encompasses multiple cycles, averaging over the small oscillations in the numerical waveform. The remaining overall trend ($t_c \approx 3660M$ to $t_c \approx 3630M$) is explained by the increasing error in the PN waveform at higher frequencies; the value $\sim 3650M$ arises because the time in the NR simulation is chosen such that $t = 0$ at the beginning of the simulation, with merger around $t \sim 4000M$. For $\delta\omega/\omega = 0.1$ (solid blue curve), residual oscillations in t_c are below $1M$, as can be seen from the inset of Fig. 3. We therefore recommend a matching width of at least $\delta\omega/\omega = 0.1$, and adopt this value for the remainder of this paper.

To the lowest PN order, the time to merger is proportional to $M\omega^{-8/3}$. Therefore, a relative frequency width of 10% corresponds to the first *quarter* of the NR waveform. The PN waveform must be sufficiently accurate throughout the entire matching interval, so this necessitates a NR waveform which extends considerably into the regime where PN errors are small.

4.3. Systematic errors in the NR waveform

Let us now examine two errors that arise during a numerical simulation: numerical truncation errors and errors introduced by gravitational wave extraction at finite radius.

We assess the truncation error by constructing hybrids from NR waveforms at three different numerical resolutions (N4, N5 and N6 in Ref. [46, 52] with approximately 57^3 , 62^3 , and 67^3 grid points respectively). These hybrids utilize a TaylorT3 PN waveform and $M\omega_m = 0.042$. We then compute $\|\delta h\|/\|h\|$ between low and medium resolution, and between medium and high resolution. Because of the rapid convergence of the spectral methods used to compute these numerical waveforms, the errors $\|\delta h\|/\|h\|$ essentially represent the error of the lower of the two resolutions involved. The results are plotted as the dashed-dotted lines in Fig. 4. Numerical truncation error is seen to be irrelevant, except perhaps at the lowest resolution. This result agrees with the results of [14] for the **Llama** code, and [27] for the **BAM** code, although [27] considers only the numerical waveform and not a hybrid.

Turning to the gravitational wave extraction at finite radius R_{GW} , we construct hybrid waveforms based on NR waveforms at two finite extraction radii, and one where the waveform is extrapolated to infinite extraction radius (we use a TaylorT3 PN waveform with $M\omega_m = 0.042$). The solid lines in Fig. 4 report the differences between the “finite-radius hybrids” and the hybrid based on the extrapolated NR waveform. The effects of finite-radius wave-extraction are significant, making even the $R_{\text{GW}} = 385M$ numerical simulation unusable for parameter estimation at moderately large ρ_{eff} . Thus, it is imperative to always utilize waveforms extrapolated to infinite extraction radius, or to use Cauchy characteristic extraction [57]. This result is of relevance to other studies such as [14], because most of the NR waveforms used in that analysis have a finite extraction radius. One should note that the results presented here are specific to the numerical waveforms we study, and may not hold in general. For example, the results from [58] show a lower error for finite extraction radius waveforms, but were obtained with a different evolution system and gauge (moving puncture BSSN, rather than Generalized Harmonic).

Wave extrapolation to infinite extraction radius is already well established [46, 59], so one might view an investigation of the impact of finite R_{GW} as less important. However, we can use the finite R_{GW} waveforms to comment on several topics of relevance.

We begin by investigating the relative importance of phase- and amplitude-errors. Using the Fourier-transforms $\widetilde{\delta h}(f)$ and $\widetilde{h}(f)$, we follow Lindblom et al. [22] and write $\widetilde{\delta h}(f) = [\delta\chi(f) + i\delta\phi(f)]\widetilde{h}(f)$, so that $\delta\chi(f)$ and $\delta\phi(f)$ represent the fractional amplitude-error and the phase-error of the waveforms in the Fourier-domain. Defining noise-weighted averages, $\overline{\delta\chi} = \|\delta\chi h\|/\|h\|$, $\overline{\delta\phi} = \|\delta\phi h\|/\|h\|$ (where $\|\delta\chi h\|$ is obtained by substituting $\delta\chi(f)\widetilde{h}(f)$ into the integral in Eq. 5), Lindblom et. al. show that

$$\frac{\|\delta h\|}{\|h\|} = \sqrt{\overline{\delta\phi}^2 + \overline{\delta\chi}^2}. \quad (28)$$

Fig. 5 plots $\overline{\delta\chi}$ and $\overline{\delta\phi}$ for three representative comparisons considered in this paper.

In the case of numerical errors the phase errors dominate over the amplitude errors, as can be seen in the left panel of Fig. 5. The right panel of Fig. 5 shows the amplitude and phase errors for a change in PN approximant and for different matching frequencies, which we will discuss in more detail in Sec. 4.4. In these cases, amplitude errors sometimes are similar to phase errors, especially for very high matching frequencies or very large total mass. In general, however, it is fair to make the assumption that phase errors dominate over amplitude errors. The discontinuity in $\overline{\delta\chi}$ and $\overline{\delta\phi}$ for one of the plotted comparisons arises because the best-fit alignment

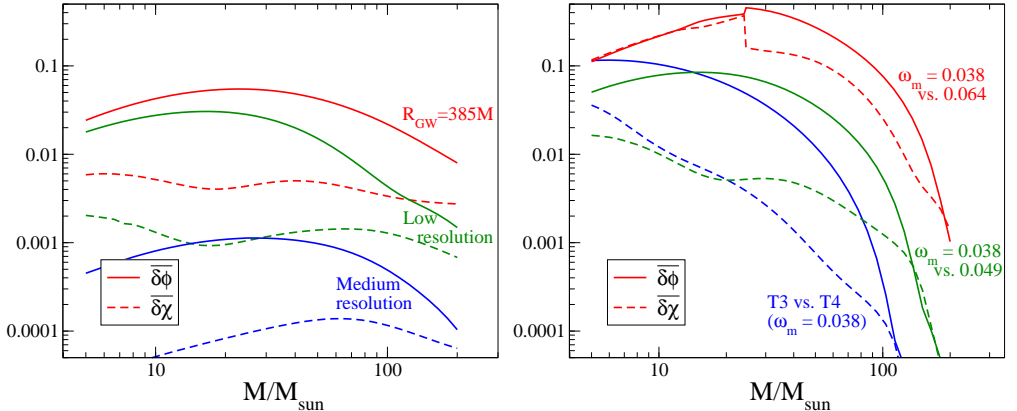


Figure 5. Contribution of amplitude- and phase-errors to the overall error $\|\delta h\|/\|h\|$. **Left:** the effect of wave-extraction at finite radius $R_{\text{GW}} = 385M$, and the effect of numerical truncation error (see Fig. 4). **Right:** the effect of a change of Post-Newtonian approximant (TaylorT3 vs. TaylorT4), and changes to the matching region ($\omega_m = 0.038$ vs 0.049 and 0.064), cf. Sec. 4.4.

between the two hybrids being compared discontinuously jumps between two local minima as M passes through a critical value where the global minimum jumps from one to the other minimum.

Next, we recall that numerical simulations are particularly susceptible to phase errors during the inspiral phase, where the energy flux is small and the inspiral time-scale is long. Finite-radius gravitational waveforms induce errors with similar properties, as can be seen in the left panel of Fig. 6, which plots the phase-errors of the finite R_{GW} numerical waveforms. Therefore, finite-extraction waveforms are a good model to assess the importance of phase-errors during the inspiral phase. Comparing the left panel of Fig. 6 to Fig. 4, we find that phase-errors of ~ 0.5 rad during the numerical simulation – whatever their origin – are not indistinguishable in advanced detectors and should be avoided.

The right panels of Fig. 6 demonstrate that the phase-errors and the respective $\|\delta h\|/\|h\|$ values are proportional to $1/R_{\text{GW}}$. This confirms our earlier assertion that $\|\delta h\|/\|h\|$ is proportional to the dominant error that enters a hybrid waveform (cf. the discussion after Eq. (10)). This proportionality allows us to predict how small numerical phase-errors should be, namely $\lesssim 0.2$ rad to be undetectable at $\rho_{\text{eff}} = 40$, and proportionally smaller for higher SNR. To include some safety margin, we recommend a target of about 0.1 rad phase error when plotted similarly to Fig. 6 as a function of frequency. The tolerable phase error during the inspiral will naturally depend on many factors, most notably the length of the NR waveform (i.e., the hybridization frequency ω_m). We have not investigated scaling with length of the NR waveform, so our recommendation only holds formally for $M\omega_m \approx 0.04$.

Fig. 7 uses the comparison between finite R_{GW} and extrapolated waveforms to motivate statements that we made in the context of Eq. (17). We plot \mathcal{M} and $(\|\delta h\|/\|h\|)^2/2$. These quantities should agree if h_{\parallel} is negligible, which indeed is the case.

Finally, Fig. 7 also shows mismatches between the pure NR waveforms (not hybridized) at finite and infinite extraction radius. These mismatches are only

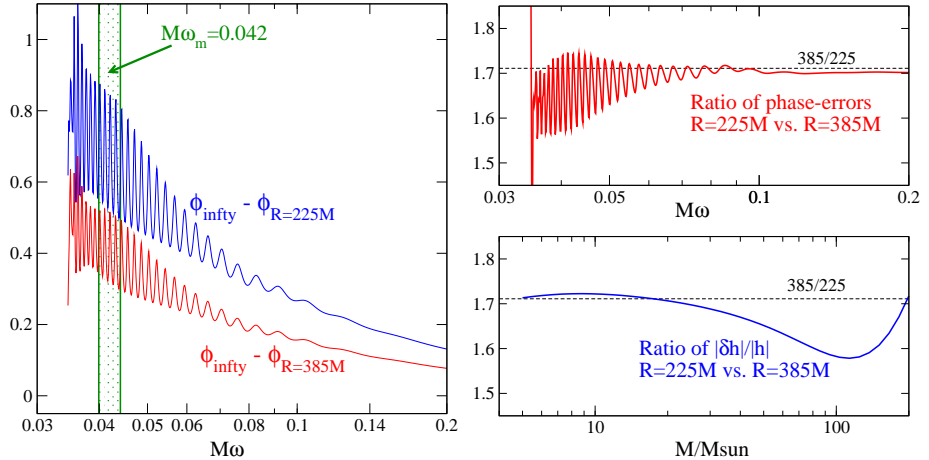


Figure 6. **Left:** Phase difference between the NR waveforms extracted at finite R_{GW} relative to a waveform extrapolated to infinite extraction radius. **Right:** “Convergence test” of finite R_{GW} waveforms with extraction radius. The top right panel shows the phase error, the bottom panel $\|\delta h\|/\|h\|$, and both are seen to decay like $1/R_{\text{GW}}$.

meaningful for sufficiently high mass M so that the NR waveform begins at frequencies, $f_{i\text{NR}}$, below the Advanced LIGO frequency band at 10Hz, i.e. for $M > 130M_{\odot}$. As expected, we see that for $M > 130M_{\odot}$ the pure NR mismatches agree very well with the hybrid mismatches, because hybridization is unnecessary and unimportant for such high masses. However, at lower masses the hybrids have much larger errors than at higher masses. The mismatch, for instance, reaches a maximum 10 times larger than the maximum mismatch of the NR-only waveforms. Therefore, one can use pure NR mismatches only to ascertain the usability of NR waveforms for high masses. Small mismatches of pure NR waveforms at high masses *do not imply* small mismatches of hybrid waveforms at lower masses. The only way to assess the quality of NR waveforms that are intended for use in hybrids lies in the construction of hybrids and computing errors based on these hybrids. Pure NR mismatches are commonly used because of their convenience (e.g., in the Samurai project [43]), but one must keep their limitations in mind.

All hybrids used in this section use the TaylorT3 PN approximant. We have repeated the calculations with other approximants without any change in our results. Our findings are, therefore, entirely due to the behavior of the numerical waveforms.

4.4. Choice of matching frequency

This section addresses at what frequency hybridization should occur, i.e., how long the NR simulations must be. There is a trade-off between computational expense and accuracy. On the one hand, we wish to match PN and NR waveforms as close to merger as possible to reduce the length and computational cost of NR simulations. On the other hand, PN waveforms diminish in accuracy toward merger. Because of its importance, this is a very active research topic [14, 27, 28].

As a first step towards understanding the importance of the matching frequency ω_m , we consider a series of hybrids where TaylorT3 is matched to the NR simulation

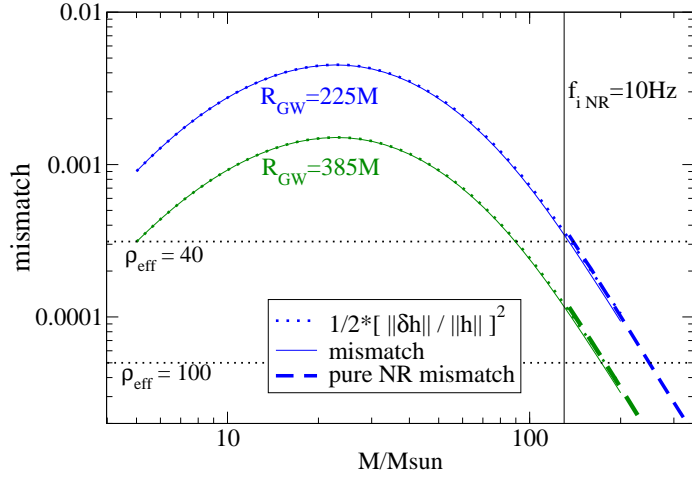


Figure 7. Verification of Eq. (15) relating $\|\delta h\|/\|h\|$ and mismatch. For the finite radius hybrids shown in Figs. 4 and 6, we plot mismatch \mathcal{M} and $(\|\delta h\|/\|h\|)^2/2$, which are virtually identical. We also plot mismatches between pure NR waveforms (no hybrids) for so high masses that the initial GW frequency of the NR waveform is $f_{i\text{NR}} \geq 10\text{Hz}$.

at different values ω_m , using a matching interval $\delta\omega = 0.1\omega_m$. We then compute the error measure $\|\delta h\|/\|h\|$ between a “reference hybrid” which is matched at the lowest possible frequency ($M\omega_m = 0.038$), and “trial hybrids”, matched at higher frequencies. The results are presented in the left panel of Fig. 8. With increasing ω_m of the trial hybrid, $\|\delta h\|/\|h\|$ becomes unacceptably large. With decreasing ω_m , $\|\delta h\|/\|h\|$ decreases, as one would expect, and for $M\omega_{\text{trial}} = 0.042$, the error criterion appears to be satisfied even at $\rho_{\text{eff}} = 40$. However, this decrease in $\|\delta h\|/\|h\|$ is a combination of two different origins. First, with earlier matching, the trial hybrid will be closer to the exact waveform, obtainable if one could match arbitrarily early, $\omega_m \rightarrow 0$. This is indeed the effect that we are trying to measure. Second, as the matching frequencies of trial- and reference-hybrid approach each other, the hybrid-waveforms themselves also approach each other, and $\|\delta h\|/\|h\|$ will decrease. To allow conclusions about the trial hybrid, we must quantify the importance of this artificial suppression of $\|\delta h\|/\|h\|$.

The right panel of Fig. 8 attempts to determine the importance of the artificial suppression due to close matching frequencies. We fix ω_{trial} , and consider decreasing values of ω_{ref} . In the limit $\omega_{\text{ref}} \rightarrow 0$, the difference $\|\delta h\|/\|h\|$ will measure the error in the trial hybrid. To reduce the dimensionality of the plot, the right panel of Fig. 8 shows the maximum of $\|\delta h\|/\|h\|$ over the mass-range $[5M_\odot, 200M_\odot]$. As expected, $\|\delta h\|/\|h\|$ becomes smaller and approaches 0 as $\omega_{\text{ref}} \rightarrow \omega_{\text{trial}}$. As was just alluded to, this is the artificial suppression of $\|\delta h\|/\|h\|$. Let us now consider the opposite limit of $\omega_{\text{ref}} \rightarrow 0$. For large ω_{trial} (for instance the top-most, magenta curve ($M\omega_{\text{trial}} = 0.064$)), $\|\delta h\|/\|h\|$ indeed levels off as ω_{ref} is made as small as possible, and asymptotes towards what appears to be some maximum value. We interpret this maximum value to represent the true error in the trial hybrid waveform if our NR waveform were arbitrarily long. For $M\omega_{\text{trial}} = 0.064$, this asymptotic value is $\|\delta h\|/\|h\| \approx 0.5$, demonstrating that a TaylorT3 hybrid matched at $M\omega_m = M\omega_{\text{trial}} = 0.064$ is not

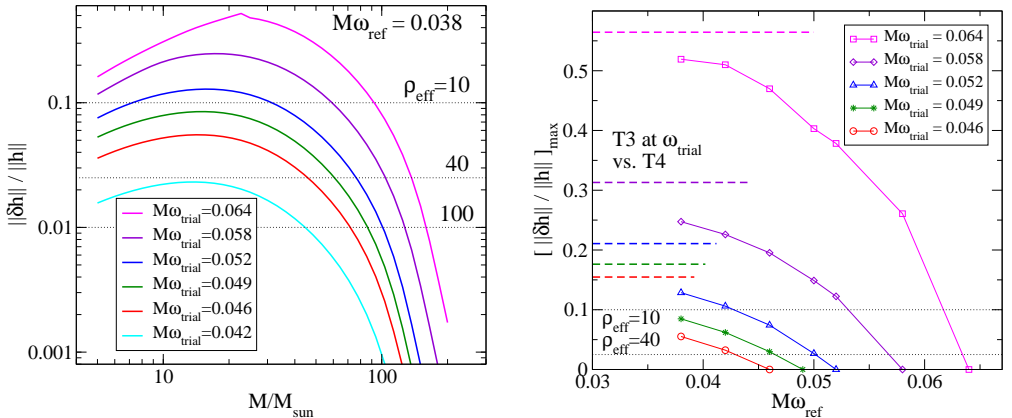


Figure 8. Errors of TaylorT3 hybrids, as a function of matching frequency ω_m . **Left:** $\|\delta h\|/\|h\|$ between matching frequencies $M\omega_{\text{trial}}$ and fixed $M\omega_{\text{ref}} = 0.038$. The dotted lines indicate upper limit of $\|\delta h\|/\|h\|$ for two different effective signal to noise ratios ρ_{eff} . **Right:** $\|\delta h\|/\|h\|$ maximized over M , as a function of the matching frequency of the reference hybrid for trial hybrids using several values of ω_{trial} . The dashed lines are the maximum values of $\|\delta h\|/\|h\|$ for each trial hybrid compared to a TaylorT4-hybrid matched at $M\omega_m = 0.042$.

useful for any data-analysis purposes.

As we move toward smaller ω_{trial} , the error $\|\delta h\|/\|h\|$ falls. Unfortunately, once ω_{trial} is so small that the error $\|\delta h\|/\|h\|$ begins to get interesting (e.g. the lowest two curves, $M\omega_{\text{trial}} = 0.046, 0.049$), the asymptotic behavior as $\omega_{\text{ref}} \rightarrow 0$ is no longer visible. In order to re-establish this behavior, we would require such a small value in ω_{ref} such that it is below the starting frequency of the numerical waveform. By utilizing only a *single* PN approximant, we can, therefore, learn only the following: the 15-orbit SpEC waveform is long enough to ascertain that matching at high frequencies $M\omega_m \gtrsim 0.055$ results in hybrids with unacceptably large errors. However, the NR waveform is too short to establish reliably the error incurred by matching at lower frequencies $0.038 \lesssim M\omega_m \lesssim 0.055$.

To gain more insight into the effects shown in Fig. 8, we explore hybrid waveforms using different PN Taylor approximants. A natural starting point involves constructing our *reference* hybrid using a PN TaylorT4 approximant, which is known to be considerably more accurate than TaylorT3 in the non-spinning equal mass case (see Ref. [46] for detailed discussion). If we assume that TaylorT4 incurs a negligible error relative to the “true” inspiral waveform, error criteria $\|\delta h\|/\|h\|$ between TaylorT4 hybrids and the previously considered TaylorT3 hybrids will display the error in the TaylorT3 hybrid. These errors are indicated by the horizontal dashed lines in the right panel of Fig. 8. (Because TaylorT4 agrees so well with NR, for convenience here we use only one TaylorT4 hybrid matched at $M\omega = 0.042$). These dashed horizontal lines in the right panel of Fig. 8 are consistent with our conclusions of the preceding paragraph: the errors in the TaylorT3 hybrids matched at high frequency ($M\omega_{\text{trial}} = 0.058, 0.064$) can be resolved by pushing ω_{ref} to the start of the NR waveform, and the asymptotic value of the TaylorT3-only comparisons agrees with those of TaylorT3—TaylorT4. For smaller ω_{trial} , we cannot reach the asymptotic regime, and while $\|\delta h\|/\|h\|$ for TaylorT3-only comparisons increases as ω_{ref} is pushed

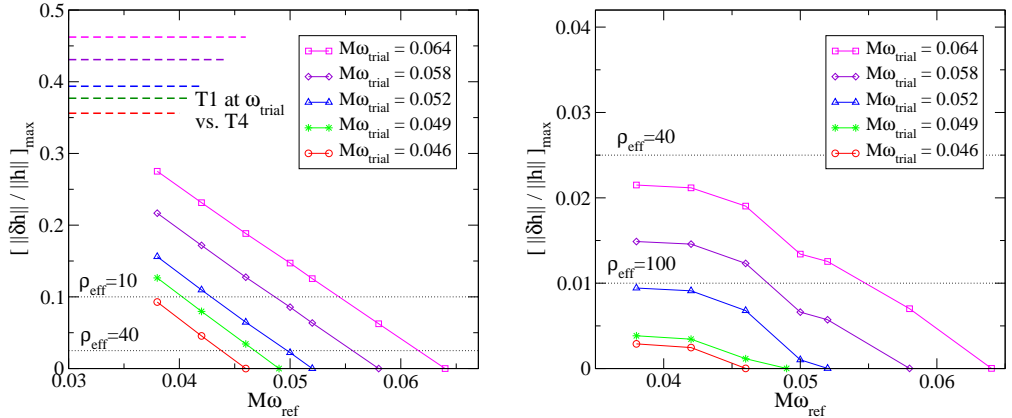


Figure 9. Left: Errors of TaylorT1 hybrids as a function of matching frequency. **Right:** Errors of TaylorT4 hybrids as a function of matching frequency. These plots mirror the right panel of Fig. 8, except using a different PN approximant (note the different y-axis scale in the right panel).

as low as possible, the error is still far away from the expected limit given by the TaylorT3–TaylorT4 comparison. The dashed TaylorT3—TaylorT4 lines indicate errors too large even for $\rho_{\text{eff}} = 10$. Under our conservative error criteria, we conclude that the NR waveform is too short to construct useful TaylorT3 hybrids.

So far, we have used the TaylorT3 PN waveform, because its analytical nature makes it the simplest to implement. We now consider different PN approximants. The left panel of Fig. 9 plots the same information as the right panel of Fig. 8, except that TaylorT3 is now replaced by TaylorT1. Similar to the right panel of Fig. 8, we can clearly see the suppression of the differences when ω_{trial} is too close to ω_{ref} . As above, this effect manifests itself in $\|\delta h\|/\|h\| \propto |\omega_{\text{ref}} - \omega_{\text{trial}}|$. However, as opposed to TaylorT3, for the TaylorT1 approximants, we do not see any indication that $\|\delta h\|/\|h\|$ levels off as ω_{ref} is made smaller, not even for the largest possible difference ($\omega_{\text{trial}} - \omega_{\text{ref}}$). Our conclusions for TaylorT1 hybrids, therefore, are identical to those reached for TaylorT3 hybrids; the current 15-orbit NR waveform is too short to construct reliable TaylorT1 hybrids on the basis of our error criteria. Or conversely, TaylorT1 is too inaccurate to be utilized with the currently available numerical waveforms within our error framework.

The right panel of Fig. 9 shows the same comparisons using the TaylorT4 PN approximant. TaylorT4 is special, in that it happens to agree very well with the numerical simulations for the equal-mass, non-spinning case. Indeed, the right panel of Fig. 9 confirms this fact; the errors $\|\delta h\|/\|h\|$ are far smaller, within our limits for detection and parameter estimation even for $\rho_{\text{eff}} = 100$ for matching frequencies $M\omega_m < 0.052$. For all ω_{trial} , convergence to an asymptotic value is visible as ω_{ref} is decreased. Therefore, TaylorT4 hybrids are suitable in the equal-mass, non-spinning case for event detection and parameter estimation. However, as is well known, this agreement is coincidental and does not carry over to more generic configurations [60]; the exceptional good behavior of TaylorT4 is, thus, not helpful for the generic case. Nevertheless, convergence towards an upper error limit at lower matching frequency suggests the suitability of different PN approximants at frequencies lower than current NR waveforms can provide.

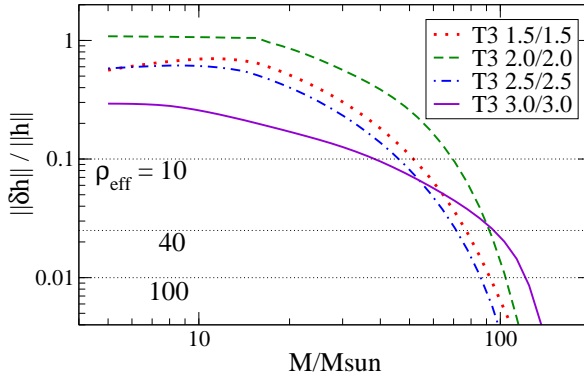


Figure 10. Error criterion evaluated between TaylorT3 hybrids at different post-Newtonian order. All hybrids matched at $M\omega_m = 0.042$, and all comparison relative to a hybrid using Taylor T3 3.5/3.0 (3.5PN order in phase, 3.0 PN order in amplitude).

We point out that our results presented in Figs. 8 and 9 are consistent with the results of Buonanno *et al.* [26] who compute overlaps for $M = 20M_\odot$ between non-hybridized Taylor approximants terminated at ISCO. Translating into our notation, they find $\|\delta h\|/\|h\| = 0.64$ when comparing Taylor T4 to Taylor T3, and $\|\delta h\|/\|h\| = 0.34$ when comparing Taylor T4 to Taylor T1. At our highest matching frequency $M\omega_{\text{trial}} = 0.064$ (which is closest to pure PN waveforms), one can read off from Figs. 8 and 9 that $\|\delta h\|/\|h\| = 0.56$ and $\|\delta h\|/\|h\| = 0.46$ respectively. This agreement is reasonably good, considering the differences in the examined waveforms.

To close this section, we briefly investigate hybrids constructed from TaylorT3 at different PN orders. We construct all hybrids at a matching frequency of $M\omega_m = 0.042$ and compute $\|\delta h\|/\|h\|$ between a reference hybrid using the most accurate PN order (3.5PN in phase, 3PN in amplitude) and trial hybrids with lower PN expansion orders. The legend of Fig. 10 indicates which PN orders we consider. All differences, even between 3.0 and 3.5PN phase accuracy, are so large, suggesting that lower order PN approximants may not be sufficiently accurate for data-analysis purposes. This finding is consistent with our earlier findings; we established earlier that using our error criteria, TaylorT3 3.5/3.0 is insufficient when matched at $M\omega_m = 0.042$. As Fig. 10 confirms, lower-order PN approximants are even less accurate, and consequently, are also insufficient within our analysis.

4.5. Effects of the noise curve

We have so far considered detection and measurement accuracies only in the context of a single Advanced LIGO interferometer. This section briefly presents $\|\delta h\|/\|h\|$ computations for different instrument noise curves including Initial LIGO (with a low-frequency cut-off of 40Hz) and a frequently used analytical fit [13] to the Advanced LIGO sensitivity curves. These noise curves are plotted in Fig. 1. The overall scale of the noise curve $S_n(f)$ and the overall scale of the waveforms $h(t)$ cancels in the normalized error criterion $\|\delta h\|/\|h\|$. Nevertheless, the shape of the waveforms and of $S_n(f)$ are important [28]. Specifically, a noise-spectrum with a wider bandwidth will be sensitive to a larger portion of the waveform.

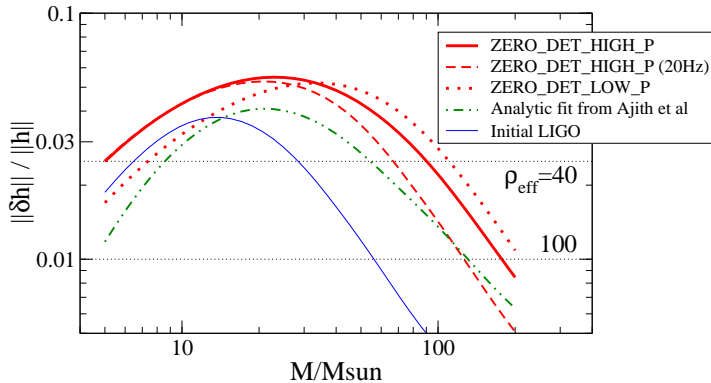


Figure 11. Effect of different noise curves on $\|\delta h\|/\|h\|$. Shown are differences between finite extraction radius $R_{\text{GW}} = 385M$ and waveforms extrapolated to infinity, cf. Fig. 4.

In order to investigate the impact of different noise curves, we use the waveform at finite extraction radius $R_{\text{GW}} = 385M$, already presented in Figs. 4–7. Fig. 11 repeats this earlier calculation for all noise curves presented in Fig. 1. The error $\|\delta h\|/\|h\|$ is larger for the larger-bandwidth noise curves, in particular `ZERO_DET_HIGH_P` and `ZERO_DET_LOW_P`. Comparing `ZERO_DET_LOW_P` and `ZERO_DET_HIGH_P`, we note that `ZERO_DET_LOW_P` is more sensitive at low frequencies relative to high frequencies, and correspondingly it results in a larger $\|\delta h\|/\|h\|$ at high masses (i.e., low-frequency waveforms) and smaller $\|\delta h\|/\|h\|$ at low masses, compared to `ZERO_DET_HIGH_P`. We also include the `ZERO_DET_HIGH_P` noise curve with a low-frequency cutoff at 20 Hz. This increased low-frequency cutoff has no impact on low mass systems with $M \lesssim 20M_{\odot}$, but results in reduced sensitivity (i.e. smaller $\|\delta h\|/\|h\|$) at larger masses, compared to the unmodified `ZERO_DET_HIGH_P` noise curve.

We note that the analytical fit to the Advanced LIGO noise curve (green line) underestimates the error $\|\delta h\|/\|h\|$ compared to the projected Advanced LIGO noise curve. Also, hybrid waveforms, sufficient for measurement accuracy with Initial LIGO, may no longer meet the same measurement criteria within an identical mass range and ρ_{eff} in the case of Advanced LIGO, as seen in Ref. [28]. Besides the larger bandwidth (which directly affects $\|\delta h\|/\|h\|$), the Advanced LIGO noise curves are more sensitive than Initial LIGO. This needs to be taken into account when choosing an acceptable ρ_{eff} . The effect of noise curve has also been studied in Ref. [14], where the error between different resolutions of NR waveforms and different types of NR codes is calculated through the Advanced LIGO and Initial LIGO noise curves. A similar trend is observed with respect to an increase in sensitivity (and therefore error) at high masses.

5. Discussion

In this paper we have presented a comprehensive study of errors that affect hybrid waveforms. We assess the quality of the hybrids based on their suitability for Advanced LIGO parameter estimation, using the criterion most recently presented in [22], and

refined in [28],

$$\frac{\|\delta h\|}{\|h\|} < \frac{1}{\rho_{\text{eff}}}. \quad (29)$$

The left-hand side of this inequality is independent of the source distance, and therefore, forms a convenient quantity for this analysis. The right-hand side incorporates the single detector signal-to-noise ratio ρ of to-be-analyzed events, a safety factor ε [28] and possibly a correction factor to account for a network of detectors, cf. Eq. (11). The inequality (29) provides a bound on ρ (or, equivalently, distance) below which the error δh is undetectable in the GW detectors, indication that h is sufficiently accurate. As argued in Sec. 2, $\rho_{\text{eff}} = 40$ is a reasonable value, on which the following conclusions are based. However, one should keep in mind that $\rho_{\text{eff}} = 100 - 250$ might be relevant if optimistic assumptions about the number of GW sources turn out to be correct, resulting in stronger accuracy demands on hybrid waveforms.

We investigated a large variety of effects that cause possible errors δh . The general theme of our findings is that Eq. (29) places strong accuracy requirements on all elements of the hybrid construction:

- (i) Section 4.1 shows that the PN waveform has to be aligned correctly to $\delta t_c \lesssim 1M$ time-offset, about 1/100 of a gravitational wave cycle.
- (ii) Section 4.3 shows that the numerical waveform must have phase-errors $\lesssim 0.1$ radians.
- (iii) Section 4.4 indicates that PN Taylor–approximants in the time domain are not sufficiently accurate when representing the inspiral waveform up to the start of currently available numerical relativity waveforms.

These three findings are interrelated. We have already pointed out in Eq. (27) that the 3.5PN order contributes a time-offset of about $t_{3.5\text{PN}} \approx 100M$ at typical matching frequencies $M\omega \approx 0.04$. The analytical formulae from the TaylorT2 approximant [29, 47] show that the 3.5PN order for an equal-mass binary contributes

$$\phi_{3.5\text{PN}} = -\frac{1}{4} \frac{357,185}{7,938} \pi (M\Omega)^{2/3} \approx -2.6 \text{ rad} \quad (30)$$

to the GW phase (at orbital frequency $M\Omega = M\omega/2 = 0.02$). Both the PN contributions $t_{3.5\text{PN}}$ and $\phi_{3.5\text{PN}}$ are much larger than the limits on the time and phase errors we established for the numerical waveforms ($1M$ and 0.1 rad, respectively), so it is unsurprising that the time-domain Taylor approximants are insufficient, or conversely, that the numerical waveforms are too short within our strict error requirements.

So how long do NR waveforms need to be in order to reliably attach a Taylor-PN inspiral? Or equivalently, how early must one stop using the PN waveforms? Fig. 12 suggests a conservative answer to this question. Both panels of Fig. 12 show the same data, but with different axes. The data presented are $\|\delta h\|/\|h\|$ for $M = 10M_\odot$ and $M = 20M_\odot$ between pairs of {TaylorT1, TaylorT3, TaylorT4} hybrids, all matched at the same frequency ω_m , and plotted as a function of hybridization frequency ω_m . Because the TaylorT hybrids only differ in their treatment of uncontrolled higher-order PN terms, these differences are a reasonable measure of the truncation error of the PN series. Fig. 12 shows that these differences are very large, far above the limit of Eq. (29). The right panel of Fig. 12 attempts power-law fits to $\|\delta h\|/\|h\|$ as a function

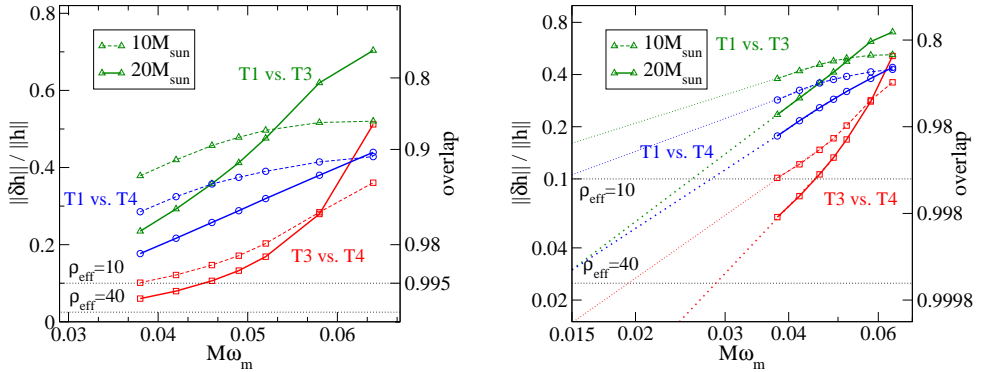


Figure 12. Differences between hybrids using different PN approximants, but matched at the same matching frequency. Plotted is the value of $\|\delta h\|/\|h\|$ at $10M_{\odot}$ and $20M_{\odot}$, as a function of ω_m . Both plots show the same data, albeit with different axes. The right plot contains power law fits to the smallest four data-points.

of ω_m . Extrapolation based on fits is highly unreliable, but nevertheless, this figure indicates that one must match at significantly lower frequencies ω_m than currently available. The time-to-merger scales in proportion to $(M\omega)^{-8/3}$, so this implies a need for NR waveforms several times longer than those currently computed.

Figure 12 shows data for total mass of $10M_{\odot}$ and $20M_{\odot}$, with the lower total mass resulting in larger $\|\delta h\|/\|h\|$. Our findings are compatible with the results of earlier PN-inspiral and EOB work [26]. In the case of the significantly lower mass (1.42, 1.38) M_{\odot} , using their faithfulness quantity, Buonanno *et al.* show that Taylor T2, T3, and T4 exhibit a corresponding $\|\delta h\|/\|h\|$ value of 0.14 with each other, whereas Taylor T1 has a somewhat worse agreement of 0.24. However, we reiterate that the criterion (29) is sufficient, and may therefore place unnecessary strong constraints on waveform accuracy.

Figure 12 clearly presents a challenge for the current state of the art in numerical and analytical waveform modelling. Fortunately, there are several potential avenues to reduce the “frequency gap” (in the language of [28]) between PN and NR waveforms.

First, one can compute longer NR waveforms. This is clearly challenging, as the following considerations based on the SpEC code illustrate. By order of magnitude, a simulation of a generic inspiral with moderate mass-ratio and spins currently requires several 10^4 CPU-hours, lasting several months. These numbers apply to an evolution time of about $5000M$ at accuracies indicated by our analysis here. Running SpEC for ~ 30 orbits is feasible, however, this will require wall-clock times approaching a year. We caution that no careful convergence tests have been performed for such simulations, though preliminary simulations appear promising. Excessive wall-clock time is the most restrictive factor in simulations longer than ~ 15 orbits. This situation can be ameliorated with at least three different approaches: increase parallelism to many more cores; utilize a faster computing architecture, e.g. graphics accelerators [61]; or develop more efficient numerical algorithms [31, 32, 33]. All three approaches are promising, and we expect that a combination of them will result in a significant extension of computational capabilities.

An alternative approach is to improve the accuracy of the PN series, either through calculation of higher PN order, or by seeking more rapidly converging

analytical representations of the inspiral phase. The EOB formalism provides such a representation, as recently argued in [28]. However, some improvements to the EOB formalism (e.g., [62]) were developed after high-accuracy NR waveforms became available for comparisons. While the improvements are well motivated on physical grounds, the additional confidence that EOB models are developed independently from the numerical results no longer applies. Finally, once one considers tuned models, one loses all ability to use differences (e.g., to the numerical result) as an error measure. Such models, by definition, will agree very well in the frequency range in which they are tuned to numerical simulations. However, such tuning does not guarantee that the cycles *before* the tuning region are well represented by the tuned model. Even with these reservations, EOB models are perhaps the most promising avenue to close the “frequency gap” between numerical simulations and Taylor post-Newtonian models.

Finally, a more detailed analysis of waveform accuracies for GW data-analysis might result in weakened requirements. The impact of detector calibration errors or of non-Gaussian detector-noise might overwhelm the limits presented here that are based on the ideal detector case. Furthermore, parameter estimation is mostly sensitive to waveform errors δh *tangential* to the signal manifold. If the errors in hybrid-waveforms are predominantly orthogonal to the signal manifold, then Eq. (29) may be overly restrictive.

In addition, let us briefly summarize how our findings impact current efforts in GW detection. The Ninja-2 project [15, 16] is well underway. This project has chosen fairly loose accuracy requirements to encourage wide participation, namely NR waveforms that must be hybridized at a frequency $M\omega_m < 0.075$, with phase accuracy of the numerical waveform better than 0.5 rad. This phase accuracy seems sufficient for event *detection* purposes (cf. Figs. 4 and 6), but matching at such high frequencies will be dominated by PN errors to a degree that would likely impact parameter estimation, (cf. Fig. 12). While the Ninja-2 project focuses primarily on event detection, some of its efforts are geared at parameter estimation. These efforts will be most useful in shedding light on the accuracy requirements discussed in this paper. Future Ninja projects may have to sharpen their accuracy requirements to avoid biasing the results by inadequate model waveforms and will likely be targeted to improve understanding of parameter estimation.

This work can of course be extended in several directions. Most immediately, our conclusions are limited by the length of the employed NR waveform, despite it being the longest published NR simulation. Therefore, it will be useful to revisit the equal-mass, non-spinning case when longer numerical data become available. Furthermore, the study needs to be extended to BBHs with different mass ratios and spins. With increasing mass ratio, the binary spends more orbits in the strong-field regime (inversely proportional to the symmetric mass ratio), so it is likely that unequal mass binaries will require yet longer numerical simulations than the equal-mass case considered here, as also pointed out by [28]. Spin effects are known only to lower PN order, so it is likely that black hole spin may necessitate longer NR simulations as well, dependent on their initial spin orientation.

Besides these obvious extensions based on refined numerical simulations, there are also conceptual questions that deserve further attention. Eq. (29) incorporates a detector network only in the crudest possible way. It would be interesting to investigate in more detail how Eq. (29) generalizes to a network of multiple detectors. More detailed investigations into accuracy standards would also be valuable. On the one hand, Eq. (29) is a sufficient condition and necessary accuracy standards for

parameter estimation may be considerably weaker. On the other hand, even when a certain error δh satisfies Eq. (29), it might nevertheless lead to systematic bias in parameter estimation [63]. One must also consider how the presence of calibration errors affects the present conclusions. Finally, throughout this paper we have applied a time and phase shift to minimize $\|\delta h\|$ between these two waveforms. This is generally acceptable, but doing so discards information about the time of merger and phase of merger of the binary. A separate study will be necessary to determine how to measure the binary's time of merger as accurately as possible, for instance, in studies of electromagnetic counterparts.

Acknowledgments

We would like to thank Michael Boyle and Nick Taylor for providing the NR waveforms that we are analyzing in this paper. We also thank Tanja Hinderer, Lucia Santamaría and Michele Vallisneri for careful reading of this manuscript. It is a pleasure to acknowledge useful discussions with P. Ajith, Mike Boyle, Duncan Brown, Alessandra Buonanno, Curt Cutler, Scott Hughes, Lee Lindblom, Frank Ohme, Ben Owen, and Larne Pekowski. H.P. gratefully acknowledges support from the NSERC of Canada, from the Canada Research Chairs Program, and from the Canadian Institute for Advanced Research. SMN's research was carried out at the Jet Propulsion Laboratory and the California Institute of Technology, under a contract with the National Aeronautics and Space Administration.

- [1] Barry C. Barish and Rainer Weiss. LIGO and the detection of gravitational waves. *Phys. Today*, 52(10):44–50, Oct 1999.
- [2] Daniel Sigg and the LIGO Scientific Collaboration. Status of the LIGO detectors. *Class. Quantum Grav.*, 25(11):114041, 2008.
- [3] F. Acernese et al. Virgo status. *Class. Quantum Grav.*, 25(18):184001, 2008.
- [4] K Kuroda and the LCGT Collaboration. Status of LCGT. *Class. Quantum Grav.*, 27(8):084004, 2010.
- [5] Prince, T. A., Binetruy, P., Centrella, J., Finn, L. S., Hogan, C. and Nelemans, G., Phinney, E. S., Schutz, B. and LISA International Science Team. LISA: probing the Universe with gravitational waves. Technical report, LISA science case document, 2007. Available as http://list.caltech.edu/mission_documents.
- [6] P. L. Bender et al. LISA - Laser interferometer space antenna for the detection and observation of gravitational waves. Technical report, Garching, Germany, 1998.
- [7] O Jennrich. LISA technology and instrumentation. *Class. Quantum Grav.*, 26:153001, Aug 2009.
- [8] J. Abadie et al. Predictions for the Rates of Compact Binary Coalescences Observable by Ground-based Gravitational-wave Detectors. *Class. Quant. Grav.*, 27:173001, 2010. arXiv:1003.2480.
- [9] Luc Blanchet. Gravitational radiation from post-Newtonian sources and inspiralling compact binaries. *Living Rev. Rel.*, 9(4), 2006.
- [10] Frans Pretorius. Binary black hole coalescence. In Monica Colpi, Piergiorgio Casella, Vittorio Gorini, Ugo Moschella, and Andrea Possenti, editors, *Physics of Relativistic Objects in Compact Binaries: From Birth to Coalescence*, volume 359 of *Astrophysics and Space Science Library*, pages 305–369. Springer Netherlands, 2009. arXiv:0710.1338 [gr-qc].
- [11] Ian Hinder. The Current Status of Binary Black Hole Simulations in Numerical Relativity. *Class. Quant. Grav.*, 27:114004, 2010.
- [12] J. M., Centrella, J. G. Baker, B. J. Kelly, and J. R. van Meter. Black-hole binaries, gravitational waves, and numerical relativity. *Rev. Mod. Phys.*, 82:3069, 2010.
- [13] P. Ajith, S. Babak, Y. Chen, M. Hewitson, B. Krishnan, A. M. Sintes, J. T. Whelan, B. Brüggmann, P. Diener, N. Dorband, J. Gonzalez, M. Hannam, S. Husa, D. Pollney, L. Rezzolla, L. Santamaría, U. Sperhake, and J. Thornburg. Erratum: Template bank for gravitational waveforms from coalescing binary black holes: Nonspinning binaries [phys. rev. d 77, 104017 (2008)]. *Phys. Rev. D*, 79(12):129901, Jun 2009.

- [14] L. Santamaría, F. Ohme, P. Ajith, B. Brügmann, N. Dorband, M. Hannam, S. Husa, P. Mösta, D. Pollney, C. Reisswig, E. L. Robinson, J. Seiler, and B. Krishnan. Matching post-newtonian and numerical relativity waveforms: Systematic errors and a new phenomenological model for non-precessing black hole binaries. *Phys. Rev. D*, 82:064016, 2010.
- [15] The NINJA collaboration. www.ninja-project.org.
- [16] B. Aylott et al. Testing gravitational-wave searches with numerical relativity waveforms: Results from the first Numerical INjection Analysis (NINJA) project. *Class. Quantum Grav.*, 26(16):165008, 2009.
- [17] The numerical relativity and analytical relativity (NRAR) collaboration. <https://www.ninja-project.org/doku.php?id=nrar:home>.
- [18] Alessandra Buonanno, Yi Pan, John G. Baker, Joan Centrella, Bernard J. Kelly, Sean T. McWilliams, and James R. van Meter. Approaching faithful templates for nonspinning binary black holes using the effective-one-body approach. *Phys. Rev. D*, 76:104049, 2007.
- [19] Alessandra Buonanno, Yi Pan, Harald P. Pfeiffer, Mark A. Scheel, Luisa T. Buchman, and Lawrence E. Kidder. Effective-one-body waveforms calibrated to numerical relativity simulations: coalescence of non-spinning, equal-mass black holes. *Phys. Rev. D*, 79:124028, 2009.
- [20] Alessandra Buonanno and Thibault Damour. Effective one-body approach to general relativistic two-body dynamics. *Phys. Rev. D*, 59(8):084006, 1999.
- [21] Mark A. Miller. Accuracy requirements for the calculation of gravitational waveforms from coalescing compact binaries in numerical relativity. *Phys. Rev. D*, 71:104016, 2005.
- [22] Lee Lindblom, Benjamin J. Owen, and Duncan A. Brown. Model Waveform Accuracy Standards for Gravitational Wave Data Analysis. *Phys. Rev. D*, 78:124020, 2008.
- [23] Lee Lindblom. Optimal calibration accuracy for gravitational wave detectors. *Phys. Rev. D*, 80:042005, 2009.
- [24] Lee Lindblom. Use and abuse of the model waveform accuracy standards. *Phys. Rev. D*, 80(6):064019, 2009.
- [25] Lee Lindblom, John G. Baker, and Benjamin J. Owen. Improved Time-Domain Accuracy Standards for Model Gravitational Waveforms. *Phys. Rev.*, D82:084020, 2010.
- [26] Alessandra Buonanno, Bala R. Iyer, Evan Ochsner, Yi Pan, and B. S. Sathyaprakash. Comparison of post-newtonian templates for compact binary inspiral signals in gravitational-wave detectors. *Phys. Rev. D*, 80(8):084043, Oct 2009.
- [27] M. Hannam, S. Husa, F. Ohme, and P. Ajith. Length requirements for numerical-relativity waveforms. *Phys. Rev. D*, 82(12):124052, 2010.
- [28] T. Damour, A. Nagar, and M. Trias. Accuracy and effectualness of closed-form, frequency-domain waveforms for nonspinning black hole binaries. *Phys. Rev. D*, 83(2):024006, 2011.
- [29] Thibault Damour, Bala R. Iyer, and B. S. Sathyaprakash. Comparison of search templates for gravitational waves from binary inspiral. *Phys. Rev. D*, 63(4):044023, Jan 2001.
- [30] Michael Boyle. The uncertainty in hybrid gravitational waveforms: Optimizing initial orbital frequencies for binary black-hole simulations. *Phys. Rev. D (submitted)*, 2011.
- [31] Stephen R. Lau, Harald P. Pfeiffer, and Jan S. Hesthaven. IMEX evolution of scalar fields on curved backgrounds. *Commun. Comput. Phys.*, 6:1063–1094, 2009.
- [32] Jorg Hennig and Marcus Ansorg. A Fully Pseudospectral Scheme for Solving Singular Hyperbolic Equations. *J. Hyperbol. Diff. Equat.*, 6:161, 2009.
- [33] Stephen R. Lau, Geoffrey Lovelace, and Harald P. Pfeiffer. Implicit-explicit (IMEX) evolution of single black holes. *In preparation*, 2011.
- [34] Samaya Nissanke. Post-Newtonian freely specifiable initial data for binary black holes in numerical relativity. *Phys. Rev. D*, 73:124002, 2006.
- [35] M Hannam, S Husa, B Brügmann, J González, and U Sperhake. Beyond the Bowen-York extrinsic curvature for spinning black holes. *Class. Quantum Grav.*, 24:S15, 2007.
- [36] Geoffrey Lovelace. Reducing spurious gravitational radiation in binary-black-hole simulations by using conformally curved initial data. *Class. Quantum Grav.*, 26:114002, 2009.
- [37] Nathan K. Johnson-McDaniel, Nicolas Yunes, Wolfgang Tichy, and Benjamin J. Owen. Conformally curved binary black hole initial data including tidal deformations and outgoing radiation. *Phys.Rev.*, D80:124039, 2009.
- [38] Lee S. Finn. Detection, measurement, and gravitational radiation. *Phys. Rev. D*, 46(12):5236–5249, Dec 1992.
- [39] Curt Cutler and Eanna E. Flanagan. Gravitational waves from merging compact binaries: How accurately can one extract the binary’s parameters from the inspiral waveform? *Phys. Rev. D*, 49:2658–2697, 1994.
- [40] David Shoemaker. Advanced LIGO anticipated sensitivity curves.

- <https://dcc.ligo.org/cgi-bin/DocDB/ShowDocument?docid=2974>, 2009. LIGO Document T0900288-v3.
- [41] B. J. Owen. Search templates for gravitational waves from inspiraling binaries: Choice of template spacing. *Phys. Rev. D*, 53:6749–6761, June 1996.
- [42] Sean T. McWilliams, Bernard J. Kelly, and John G. Baker. Observing mergers of nonspinning black-hole binaries. *Phys. Rev. D*, 82:024014, 2010.
- [43] Mark Hannam, Sascha Husa, John G. Baker, Michael Boyle, Bernd Bruegmann, Tony Chu, Nils Dorband, Frank Herrmann, Ian Hinder, Bernard J. Kelly, Lawrence E. Kidder, Pablo Laguna, Keith D. Matthews, James R. van Meter, Harald P. Pfeiffer, Denis Pollney, Christian Reisswig, Mark A. Scheel, and Deirdre Shoemaker. The Samurai Project: verifying the consistency of black-hole-binary waveforms for gravitational-wave detection. *Phys. Rev. D*, 79:084025, 2009.
- [44] K. G. Arun, Alessandra Buonanno, Guillaume Faye, and Evan Ochsner. Higher-order spin effects in the amplitude and phase of gravitational waveforms emitted by inspiraling compact binaries: Ready-to-use gravitational waveforms. *Phys. Rev. D*, 79(10):104023, May 2009.
- [45] Lawrence E. Kidder. Using full information when computing modes of post-Newtonian waveforms from inspiraling compact binaries in circular orbit. *Phys. Rev. D*, 77:044016, 2008.
- [46] Michael Boyle, Duncan A. Brown, Lawrence E. Kidder, Abdul H. Mroué, Harald P. Pfeiffer, Mark A. Scheel, Gregory B. Cook, and Saul A. Teukolsky. High-accuracy comparison of numerical relativity simulations with post-Newtonian expansions. *Phys. Rev. D*, 76:124038, 2007.
- [47] Thibault Damour, Bala R. Iyer, and B. S. Sathyaprakash. Comparison of search templates for gravitational waves from binary inspiral: 3.5PN update. *Phys. Rev. D*, 66(2):027502, Jul 2002.
- [48] John G. Baker, Sean T. McWilliams, James R. van Meter, Joan Centrella, Dae-II Choi, Bernard J. Kelly, and Michael Koppitz. Binary black hole late inspiral: Simulations for gravitational wave observations. *Phys. Rev. D*, 75:124024, 2007.
- [49] Alessandra Buonanno, Gregory B. Cook, and Frans Pretorius. Inspiral, merger, and ring-down of equal-mass black-hole binaries. *Phys. Rev. D*, 75(12):124018, 2007.
- [50] Mark Hannam, Sascha Husa, José A. González, Ulrich Sperhake, and Bernd Brügmann. Where post-Newtonian and numerical-relativity waveforms meet. *Phys. Rev. D*, 77:044020, 2008.
- [51] <http://www.black-holes.org/SpEC.html>.
- [52] Mark A. Scheel, Michael Boyle, Tony Chu, Lawrence E. Kidder, Keith D. Matthews, and Harald P. Pfeiffer. High-accuracy waveforms for binary black-hole inspiral, merger, and ringdown. *Phys. Rev. D*, 79:024003, 2009.
- [53] Tony Chu, Harald P. Pfeiffer, and Mark A. Scheel. High accuracy simulations of black hole binaries: spins anti-aligned with the orbital angular momentum. *Phys. Rev.*, D80:124051, 2009.
- [54] Bela Szilágyi, Lee Lindblom, and Mark A. Scheel. Simulations of Binary Black Hole Mergers Using Spectral Methods. *Phys. Rev. D*, 80:124010, 2009.
- [55] R.B. Blackman and J.W. Tukey. *The Measurement of Power Spectra, From the Point of View of Communications Engineering*. Dover Books, New York, NY, first edition, 1959.
- [56] D.J.A. McKechn, C. Robinson, and B.S. Sathyaprakash. A tapering window for time-domain templates and simulated signals in the detection of gravitational waves from coalescing compact binaries. *Class.Quant.Grav.*, 27:084020, 2010.
- [57] C. Reisswig, N. T. Bishop, D. Pollney, and B. Szilágyi. Unambiguous Determination of Gravitational Waveforms from Binary Black Hole Mergers. *Physical Review Letters*, 103(22):221101, November 2009.
- [58] Mark Hannam, Sascha Husa, Franke Ohme, Doreen Müller, and Bernd Brügmann. Simulations of black-hole binaries with unequal masses or nonprecessing spins: Accuracy, physical properties, and comparison with post-Newtonian results. *Phys. Rev. D*, 82:124008, 2010.
- [59] M. Boyle, A.H. Mroué. Extrapolating gravitational-wave data from numerical simulations. *Phys. Rev. D*, 80:124045, 2009.
- [60] Mark Hannam, Sascha Husa, Bernd Brügmann, and Achamveedu Gopakumar. Comparison between numerical-relativity and post-Newtonian waveforms from spinning binaries: the orbital hang-up case. *Phys. Rev. D*, 78:104007, 2008.
- [61] Abdul H. Mroué. Binary black hole simulations using CUDA. NVIDIA GPU Technology Conference, 2010.
- [62] T. Damour, B. R. Iyer, and A. Nagar. Improved resummation of post-Newtonian multipolar waveforms from circularized compact binaries. *Phys. Rev. D*, 79:064004, 2009.
- [63] C. Cutler and M. Vallisneri. LISA detections of massive black hole inspirals: Parameter

extraction errors due to inaccurate template waveforms. *Phys. Rev. D*, 76(10):104018, November 2007.